processes

IMPACT FACTOR 3.5

CITESCORE 4.7

Review

A Review on the Use of Active Power Filter for Grid-Connected Renewable Energy Conversion Systems

Dipak Kumar Dash and Pradip Kumar Sadhu

Special Issue

Power Electronics for Energy Transition and Renewable Energy Conversion Processes

Edited by

Dr. Matías Díaz and Prof. Dr. Jose Rodriguez

MDPI

https://doi.org/10.3390/pr11051467

processes

MDPI

Review

A Review on the Use of Active Power Filter for Grid-Connected Renewable Energy Conversion Systems

Dipak Kumar Dash * and Pradip Kumar Sadhu

Department of Electrical Engineering, IIT(ISM), Dhanbad 826004, India; pradip@iitism.ac.in
* Correspondence: dipak.nitrkl@gmail.com

Abstract: Renewable energy sources such as photovoltaic (PV) and wind energies are integrated into the grid due to their low global emissions and higher power conversion efficiency techniques. Grid-connected inverters are the core components of distributed generation networks. However, several harmonic current and voltage variations affect the performance of circuits in grid-connected networks. These issues can be easily resolved using passive filters, static vector generators, and dynamic energy filters (APFs). In higher-level units, the cost, dimensions, and weight of passive filters increase proportionally. The purpose of this research is to evaluate advanced APFs for reducing power switches and grid-connected weight, cost, and scale. Several studied APF inverter topologies, including single-phase, three-phase AC–AC, back-to-back, and common parameters, have been considered. Cost-effective solutions such as PV-based transformers based on APF, fewer inverters, multiple and multifunctional inverters, and wind-assisted conversion systems have been studied.

Keywords: APF; inverter; PV; WECS; power quality

Citation: Dash, D.K.; Sadhu, P.K. A Review on the Use of Active Power Filter for Grid-Connected Renewable Energy Conversion Systems. *Processes* **2023**, *11*, 1467. https://doi.org/10.3390/pr11051467

Academic Editors: Matías Díaz and Jose Rodriguez

Received: 24 March 2023
Revised: 23 April 2023
Accepted: 27 April 2023
Published: 12 May 2023

1. Introduction

In contemporary developments, the demand for electricity from households to businesses is increasing swiftly, reducing energy supply and leading to network outages. To maximize energy production and efficiency and dependability have led to the implementation of distributed electricity [1,2], such as PV systems [3], optimization [4], energy storage [5], wind turbines [6,7], fuel cells [8], distributed power systems [9]. PV and wind energy are two of the most important renewable energy sources for reducing the demand on the national utility and the global environment.

However, the integration of PV and wind power into the grid generates a certain level of harmonic, heat, and other difficult problems in terms of quality and other energy issues. These issues have a negative effect on the variation of the current and voltage sine waves [10], leading to decreased system performance [11], transformer overheating, increased motor and cable malfunction, and increased power loss [12]. To make the solar grid system more reliable, necessary harmonic and energy reduction techniques must be implemented. Various solutions for power quality issues [13] have been proposed, including unbalanced power grids, load equilibrium, harmonic injection, unavoidable neutral current, reactive power load, and electrical device intervention. In grid-integrated applications, filters are commonly combined with a passive filter to combat serial harmonic systems.

However, passive filters are constrained by issues such as limited filters, certain load ranges, fixed compensation, large grid sizes, and negative grid and series impedances [14–17], which enable the passive components to degrade rapidly [18]. In examinations of interconnected devices such as wind turbines and inverters [19], advanced filtering technologies such as a static sync compensator, an active power filter (APF), a dynamic voltage meter, multistage inverters, and a consistent power quality control system will be discussed. The APF shunt is the most widespread and permissive method for this (SAPF). The basis of filter efficiency is the current filters, inverter parameters, and controller [20,21]. The APF is

effectively regulated by p-theory, straightforward positive sequences, and synchro [22] detection. Currently, techniques for harmonic load detection are used to generate a reference signal. International standards such as IEEE-59 [23,24] and IEC a 61000-3-2 [25] impose constraints on the design and operation of electricity utility networks. In addition, the APF rating [26] is increasing in terms of demand for loads, power accumulation, and prices. For SAPF and PF customization, hybrid APF (HAPF) [27] is used. To eradicate low-order harmonics, the HAPF is powered by both SAPF [28] filters and PF for high-frequency harmonics [29]. APFs reduce load disturbances and increase compensation for harmonic voltage and current. The part of power filters based on power rating and faster response is depicted in Figure 1.

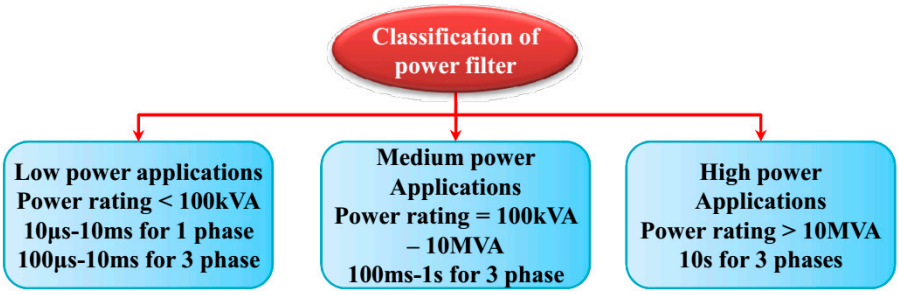

Figure 1. Subdivision of power filter based on power rating and speed of response.

However, a reduced transformer topology results in cleaner and more stable units, smaller volume capacities [30], lower costs [31], and more compact systems [32] than older topologies. Table 1 provides a fast comparison of the topologies of various grid-connected PV systems. The total cost of the device is weighed against three issues: a galvanic link [33], a fluctuation in the net voltage of the input pole to the ground [34], and safety, as well as transmission cost and system efficiency [35–38].

Table 1. Analysis of APFs in the grid-interconnected scheme.

Ref.	Methodology	Control Scheme	Capacity	Switching Frequency (kHz)	THD (%)	DC Link Voltage	Interconnected Grid Scheme
			Single-Phase Topology				
[14]	Four-bridge	SPWM/PI	≤2 kVA	18	2.83	160 V	PV-Grid-APF
[16]	Full-bridge	SPWM/PI	1.5 kVA	20	4.2	240 V	PV-Grid-APF
[17]	Full-bridge	SPWM/PI	≤1.3 kVA	16.4	<3	250 V	PV-Grid-APF
[18]	Four-bridge	Hysteresis	1.1 kVA	-	<3	230 V	PV-Grid-APF
[19]	Full-bridge	SPWM/PI	3 kVA	-	2	400 V	PV-Grid-APF
[21]	Full-bridge	SPWM/Lyapunov	3.4 kVA	20	2.49	240 V	PV-Grid-APF
			Three-Phase Topology				
[28]	H-bridge	Hysteresis	1.3 kVA	16	1.35	240 V	PV-Grid-APF
[31]	Four-bridge	SPWM/PI	10 kVA	12	2.5	360 V	PV-Grid-APF
[30]	Full-bridge	SPWM/PI	7.6 kVA	10	3.6%	340 V	PV-Grid-APF
[35]	4L-NPC	SPWM/TCL	10 kVA	8	4.36%	360 V	PV-Grid-APF

The alternating current network power is utilized by electrical transmission systems and loads [39], whereas the direct current (DC) drives the green energy outgoing voltage. In both stand-alone and network-connected systems, an inverter is necessary to convert alternating current (AC) electricity into direct current (DC). It is utilized to generate an alternating current output with a sinusoidal waveform using the same collection of electronics, ranging from low power KW to high power MW [40,41]. Inverters are actively being designed and are extremely useful for large-scale wind and photovoltaic applications. Despite demand, most power-switching components, such as IGBTs and metal oxide field effect bipolar transistors, pose a significant challenge for converters (MOSFETs). Many pure

SAPFs are minimized by using the higher power classification elements to improve the correction of the utility component and current harmonic compensations. As the system becomes more related to the grid, the increase in semiconductor switching components causes more switch losses, contributes to harmonic waveform power output voltage, lowers system efficiency [42], and defines system efficiency [43]. State-of-the-art solution in power electronics such as power semiconductors, circuit, sensor, and control circuit has recently been developed with reduced switch counting [44]. Although the reduction in components is essential in advancing energy problems, there is little literature regarding the reduction in APFs. The extensive research indicates progress in APF switching reduction and emphasis on grid-connected inverter cost, size, and weight loss. This document includes a comprehensive, systematic analysis of the literature by experts on reduction mechanisms and power transmission systems for grid-linked photovoltaic and wind energy systems. For PV APFs and WECS, some areas of research include module reduction, fewer inverters, and multispeed multifunctional inverters (ML-MFIs). In comparison to existing THD-based topologies, harmonic mitigation, active and reactive power adjustment, component speeds, and benefits, the new topology is more efficient and offers more advantages. Researchers are paying little attention to the study, which is being utilized to create and test more switching prevention approaches.

The paper consists of following sections, of which the first is an outline. In Section 2 grid-connected PV and WECS systems on issues of power quality are discussed. Section 3 shows the fundamental and recent development of APF topology and the fundamental properties of the topology. The effects of such topologies are reviewed and compared in Sections 4 and 5. A brief comparison of SAPF technology is also made. Sections 6 and 7 considers compensation techniques. Section 8 discusses the overall control techniques. Section 9 gives an overall discussion. Section 10 summarizes the outcomes in conclusions and future directions.

2. Harmonics Mitigation and Distributed Device Generation

2.1. Grid-Synchronized APF-PV Based Inverter

The main goal of installing a PCC (point of common coupling) [45] is to improve the operation and efficiency of power delivery systems. In interactive PV grid topologies, it is common to pair a PV inverter with an SAPF (active power filter) [46] and a voltage and reactive control superstation in order to prevent the costs of the power circuit from rising too high. The PV inverter converts the electricity produced by the solar photovoltaic device into usable electricity, while also filtering the harmonics of the load current [47–49]. Integrating an APF into the grid-connected PV system enhances its performance, reliability, and reduces current harmonic distortions [50–56].

A recent evaluation places the ML-MFI (multispeed multifunctional inverter) at the top of the list of innovative power generation technologies that have been incorporated into the PV grid. PV and magnetic field induction are two of these devices. By using harmonic distortion measurements that are kept to a minimum while working at a high DC–rated voltage, the output waveform is clear and free of distortion. Multifunctional inverters must handle several issues, including grid power and imbalance harmonic mitigation, reactive energy compensation, PCC voltage [57,58], and the period between PV and power grids during APF operations.

Table 2 analyzes reactive power compensation in grid-integrated PV inverter setups and additional APF functions. In references [59,60], PWM (pulse-width modulation) space-vector twist-driven technology is used to build a three-level PV system with an SVSPWM (space-vector pulse-width modulation) for effective grid filtering [61], compensatory management, and power balancing [62].

SAPF provides harmonic removal for the PV-harmonic network and a process for compensating for reactive energy to keep a constant voltage throughout the DC connection [63]. An acceptable statistical model is required to have controls that are more isolated from the variance of parameter values [64]. Energy storage devices such as batteries, super

capacitors, and flywheels are made to handle the intermediate issues that arise in a solar photovoltaic system. Due to the inherent characteristics of photovoltaic systems, the rate of electricity generation can fluctuate, which can have a detrimental impact on the network's effectiveness. Energy storage devices help maintain a constant voltage [65], lower voltage fluctuations [66], and improve solar panel efficiency [67]. The optimized PV grid system performance also leads to a reduction in harmonic content and better reactive potential control.

Table 2. Parameters of reactive power compensation control impacted devices.

Parameters	RC Bank	AVC	DBR	SDBR	STATCOM	SVC	TCSC	UPQC
Voltage Stability	###	##		#	###	##	#	####
Flicker	#	##	#		#	###	##	####
Power Flow	#	##			###	#	-	####
Oscillation Damping	#	-			###	##	###	####
Active Power	-	-	#	#	###	-	#	####
Harmonic Reduction	#	#	#	#	#	#	-	####

Symbolizes the effectiveness of the technique.

2.2. Wind Energy APF Grid-Interlinked

Recently, the use of renewable energy has risen in importance within the energy industry. With time, wind energy has improved in terms of legality, cost, and usability [68]. With no greenhouse gas emissions, a progressive, open, and scalable clean energy supply that guarantees that electricity demand is met and a more environmentally friendly energy distribution network, wind energy is also more affordable than fossil fuels and solar energy [69]. It is also more cost-effective than both of these sources of energy. However, achieving a power economy in grid-connected WECS is a challenging issue. The necessity for WECS installation with the main grid has an impact on reactive control, voltage spikes, switching, and flickering, as well as power and performance at the PCC during operations. Basic functions of variable speed in WECS include active regulation, reactive regulation, and the comparability of nonlinear and unbalanced loads. Nonlinear-control devices [70], which increase thermal efficiency while decreasing system efficiency, result in excessive tension, current, and WECS output degradation [71], as well as decreased WECS 4durability [72]. To accomplish even greater energy efficiency, WECS uses a network of harmonic reduction and reactive power compensation technologies [73]. When operating an APF to reduce existing harmonics, a WECS gives the PMSG for continuous wind speed [74]. An upstream modified modulation method based on various signal extraction techniques is used to control an APF device. To eliminate the harmonics and serve as APF in an island mode, a WECS [64] variable frequency-based technique is used that is even more sophisticated. WECS used electricity from APF in insulating mode by employing a fixed-rpm doubly fed induction generator (DFIG). To minimize conversion costs, the WECS approach employs a reduced-count topology [75]. The back-to-back converters in this area of voltage imbalance are split capacitors. In this configuration, there are issues with the separation between the grid and several PMSGs. It is necessary to add more DC connection condensers, increase the voltage significantly, and raise the semiconductor stress [76]. Reactive capacity monitoring and offsetting, a crucial component of the power supply system, are included in the networked WECS. To prevent losses in the transmission of reactive electricity to the power grid, it is essential to keep a constant voltage profile. The load tap changer transformer is one of the most crucial parts of the grid's reactive energy compensation mechanism. Additionally, many WECS produce low volts and reactive power in a combined induction generator [77]. Solutions include STATCOM, SVC, on-load tap shifters (OLTCs), transformer condensers, PWM inverters, and condenser and inductor combinations [78]. DBR, OLTC, and manually switched condensing systems are some examples of technologies that are unable to overcome harmonics and voltage gaps. SVC, STATCOM, and DFIG systems have been added to fixed-speed wind turbines to increase their reactive output

and dynamic stability [79]. By preserving the voltage equilibrium [76], these technologies enable grid-connected networks to use more wind energy. The WECS network is connected to the power-compensating systems. In Table 2 Reactive power compensation systems such as automatic voltage control (AVC), on-load tap changers (OLTC), dynamic voltage regulators (DERS), SBBR, STATCOM, static VAR controls (SVC), and thyristor-controlled sequencing (TCSC) are compared.

3. Taxonomy of Grid Connected APF

The topology, converter form, and various stages of APFs are generally categorized as shown in Figure 2 [80]. The three categories are the three subclasses of the mythology classification, SAPF, APF, and HAPF. The phase number is represented by the single (two wires), three (three cables), and four (four cables). [81] The three subclasses of shunts, sequences, and hybrids that rely on topology are shown in Figure 3. The APF series improves electrical terminal supplies by reducing the negative chain of harmonic voltage propagation caused by unit resonance [82]. The energy sector presently lacks ratings and has a small filter size due to the rising demand for high-current energy. In Table 3, the three APF structures [83,84] are compared. Three different HAPF circuit variants are depicted in Figure 3. The APF series with shunt PF offers a high level of insulation in the medium voltage configuration, as shown in Figure 3c Reactive power, voltage correction, and harmonic balance are all provided for three-phase voltages [85–87]. As depicted in Figure 3b, SAPF, in conjunction with a PF shunt, removes the harmonics of single reactive power and load current [88,89]. The expense of switching reactive power compensation has decreased for both high-performance solutions [90–93]. The APF and Shunt PF Series effectively lower unit volume and costs while maintaining constant DC connection voltage and basic grid voltage in medium- and high-voltage applications [94–97], as shown in Figure 3a. Limitations of shunt APF are energy losses and the requirement of high rating capacitors.

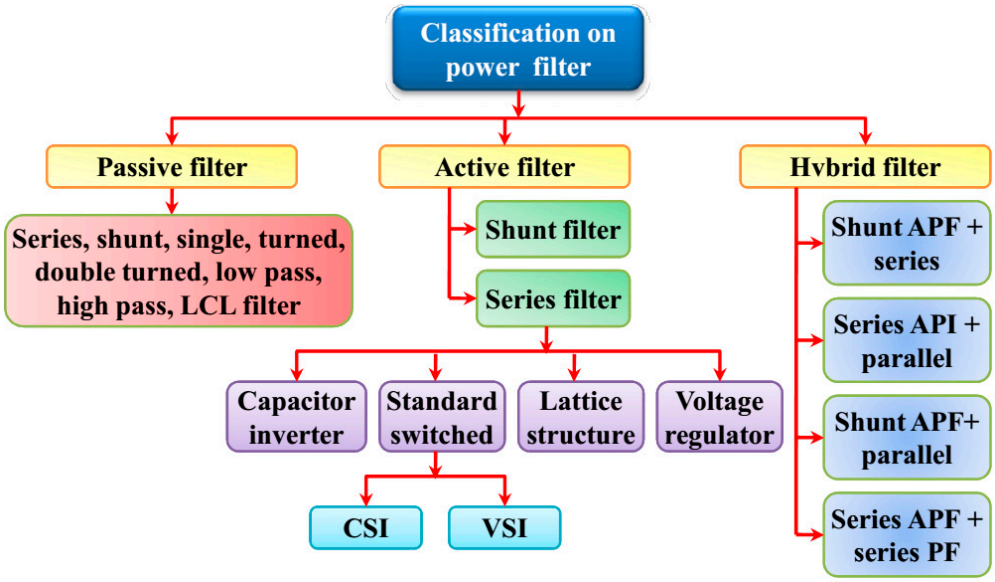

Figure 2. Subdivision of Power Filters.

Limitations of series APF as complex control algorithm and can be used for moderate frequencies. The limitation of hybrid APF is its initial cost but its efficiency is more as compared to the other two APFs.

Table 3. Methodologies of AC–AC Inverters with Reduced Switch Counts are Compared.

Schemes/Methodology	References			
	[80]	[83]	[90]	[97]
Methodology	One arm	Three arm	Two Arm	Two Arm
Capacity (kVA)	3.6	4	2.4	2.7
Switching frequency (kHz)	4	5	6	12
Reduced switch count	2	3	3	2
Grid voltage (V)	220	205	110	220
THD%	4.2	3.6	3.45	2.8
Probable Efficiency	High	Low	Medium	Medium
DC linked voltage (V)	220	320	240	110

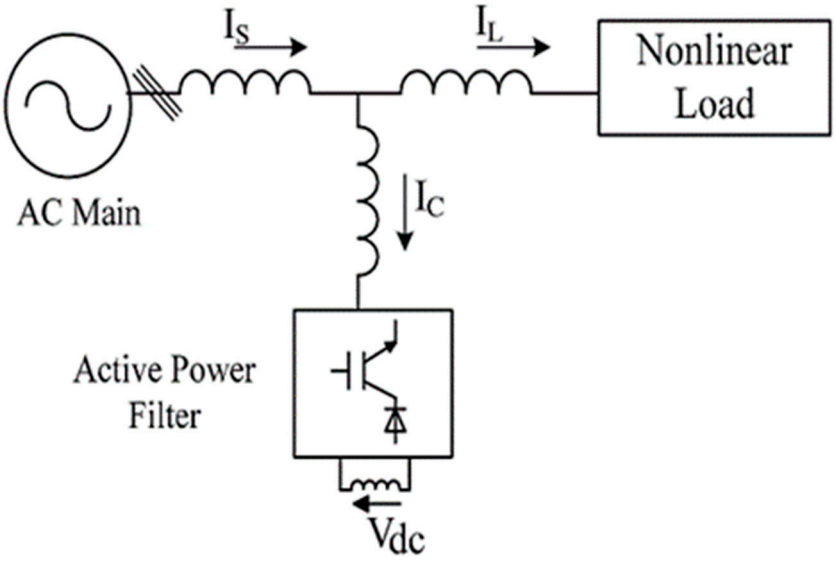

(**a**)

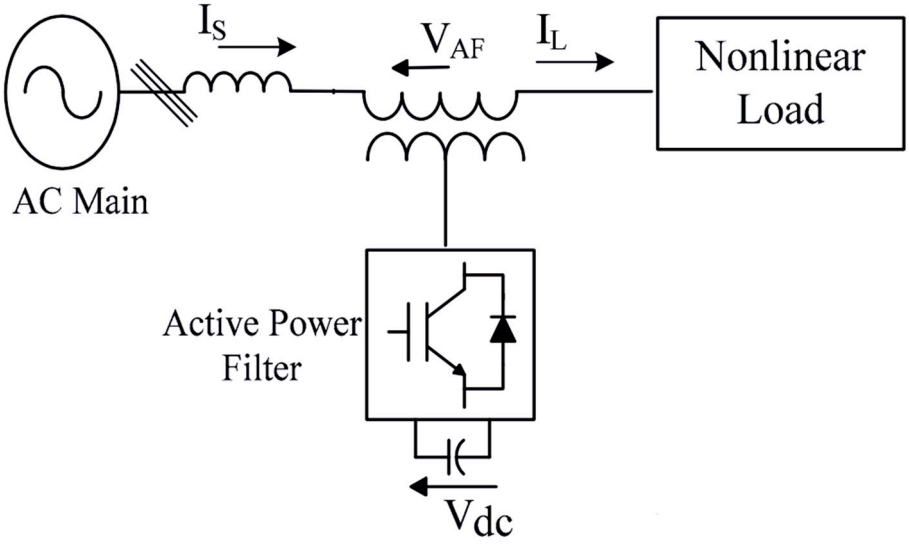

(**b**)

Figure 3. *Cont.*

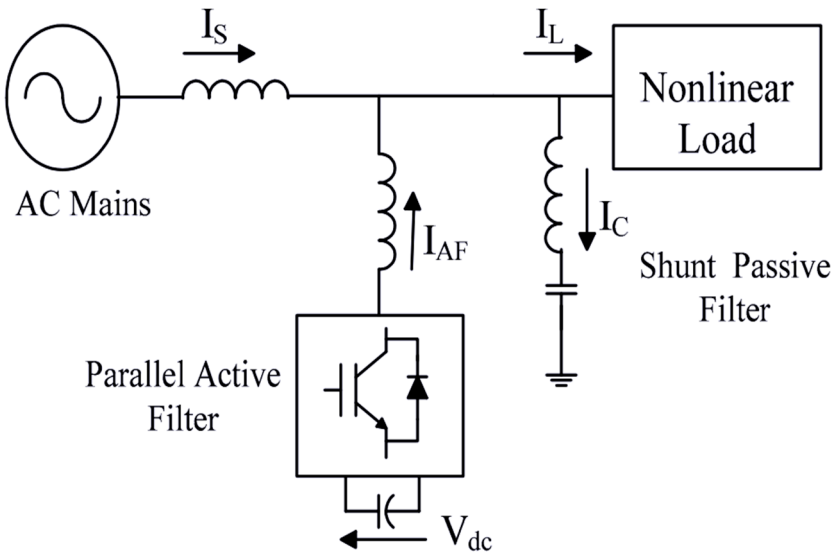

(**c**)

Figure 3. (**a**) Shunt APF, (**b**) series APF, and (**c**) hybrid APF [82].

4. Reduced APF-Inverter Topologies: A Comparative Study and Regulation

The AC–AC inverter, back-to-back inverter, and normal inverter topologies are explored in this study to determine which topologies have the optimal APF settings for reducing turn counts. When using the grid architecture, the whole interconnected switch count spectrum between 12 and three switches is shown in Figure 4.

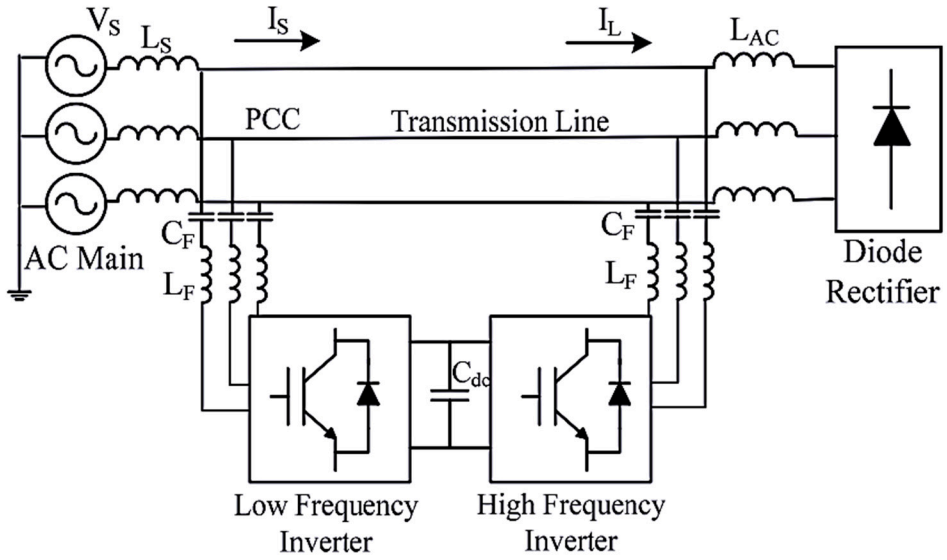

Figure 4. AC–AC inverter topology [20].

4.1. Topology of AC–AC Inverters

The AC–AC inverter topology is attached to a DC-like condenser in parallel with the pulse width modulating the voltage inverter, as seen in Figure 4. AC–AC inverter arrangements are similar in phase, three-phase three-wire, and three-phased four-wire systems.

4.2. APFs with Two Wires (Single Phase)

In high-power systems, diode-clamped, fly-volume and switch-clamped inverters utilize an assortment of semiconductor switches to produce their output. Harmonic reduction, reactive power compensation, and inverter failure characteristics are all provided by

the single-phase six-switch reduced-count VSI, which does not require fastening diodes or floating condensers. A five-tier, eight-switch transformer can transform the terminal voltage of alternating current without the need for a transformer. The two airborne condenser units are accountable for the precise volume control, the unit's weight, and the cost of reducing the voltage pressure. The topologies of four distinct inverter configurations are summarized in Table 4. Nine-switch AC–AC inverter APF circuit is mentioned in Figure 5 [88].

Table 4. Topologies of AC–AC Inverters with Reduced Switch Counts.

Schemes/Methodology	References			
	[81]	[83]	[90]	[97]
Methodology	H-bridge	Four arm bridge	Full bridge	H-bridge
Capacity (kVA)	3	4.3	12	10
Switching frequency (kHz)	10	10	12	10
Reduced switch count	6	8	6	6
Grid voltage (V)	220	220	110	110
THD %	4.7	1.5	1.22	1.25
Probable Efficiency	Medium	Low	Medium	High
DC linked voltage (V)	30	110	220	110

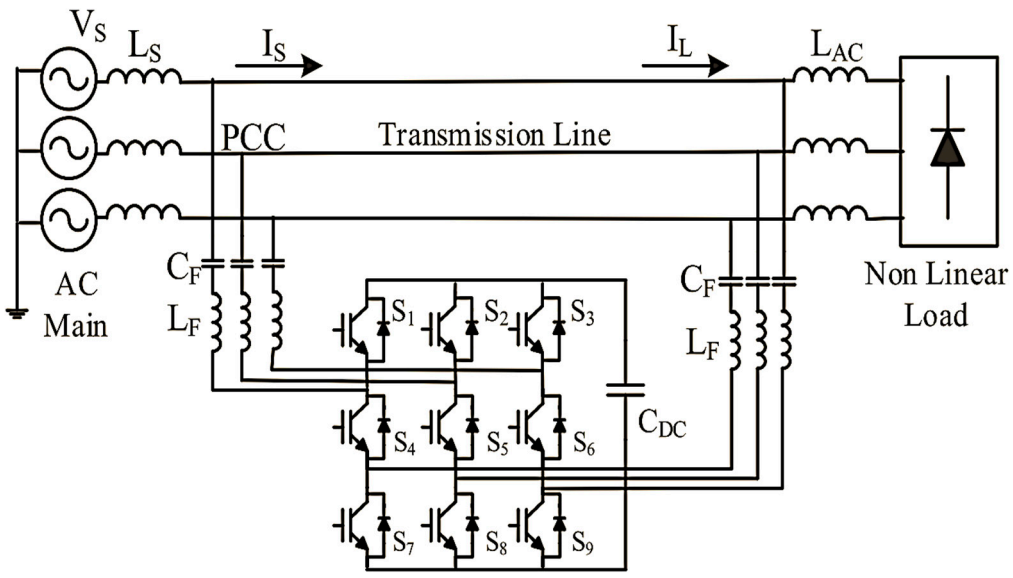

Figure 5. Nine-switch AC–AC inverter APF circuit [88].

For three-stage inverter bootstrapping technology, both an isolated multi-DC supply and an electrolyte condenser are required. Both circuit switches are connected to the same source or transmitter in order to reduce gate drive energy supplies to a single source. Due to its larger size, an electrolytic condenser has a reduced lifespan. A single-stage three-phase converter contains less harmonic material in comparison to a two-stage converter. The requirement for a distinct DC source decreased modularity and decreased fault tolerance are three disadvantages [90]. However, a reduction in the part's voltage and an increase in the system's power factor significantly reduce unit cost, switching delays, and state changes. To minimize costs [98], the transformer-less transformer line for the banking battery control and DC current and AC power output is available at interactive continuous power supplies (UPS). A DC driver is connected in series with a three-leg transformer serving as a buffer, a set of filter condensers, a set of filter inductors, and batteries. There are four and eight converters in a three-phase APF configuration. It employs a two-arm inverter bridge, a DC linking condenser, and a normal mode current technique to halt the DC-Link voltage fluctuation resulting from harmonic reactive power issues in numerous

applications [99]. The only disadvantage of the three-phase APF is that high-voltage switches are required due to high-resistance switches. When DC-bus voltage was reduced by half, soft-switching converters [100] increased total power. Compared to a conventional three-stage transformer, the PWM controller has four MOSFETs, one floating condenser, and magnet nodes with two-clamp diodes, which reduces the transformer's size and cost. The two centrally taped correction units reduce the current rates of rectification diodes, output filter inductors, and transformer turns by testing the output voltage to execute and recirculate switching operations. The result is a reduction in demand power sharing, a reduction in voltage transition burden, and zero voltage switching (ZVS). Within a conventional three-phase matrix converter, the 18 IGBT switches have sophisticated switching mechanisms. IGBT reduced-count converters are utilized by fifteen switches as mentioned in [101]. With 12 IGBT switches, an unusually sparse matrix converter with a reduced number of switches [102] generates a unidirectional power flow. The more efficient six-leg inverter is used to surmount the three-leg limitation of [89]. Figure 6 depicts the HAPF topology in three phases without the transformer, which consists of a six-way double-switch inverter with two LC filters affixed in series. In three phases, the harmonic frequency exceeds both the HAPF and VSI topologies. In addition, as shown in Figure 4, the one-leg inverter influences two half-bridge inverters with at least three distinct condensers. Two complete and medium-range converters are wired to single- and three-phase loads on each of the two modules.

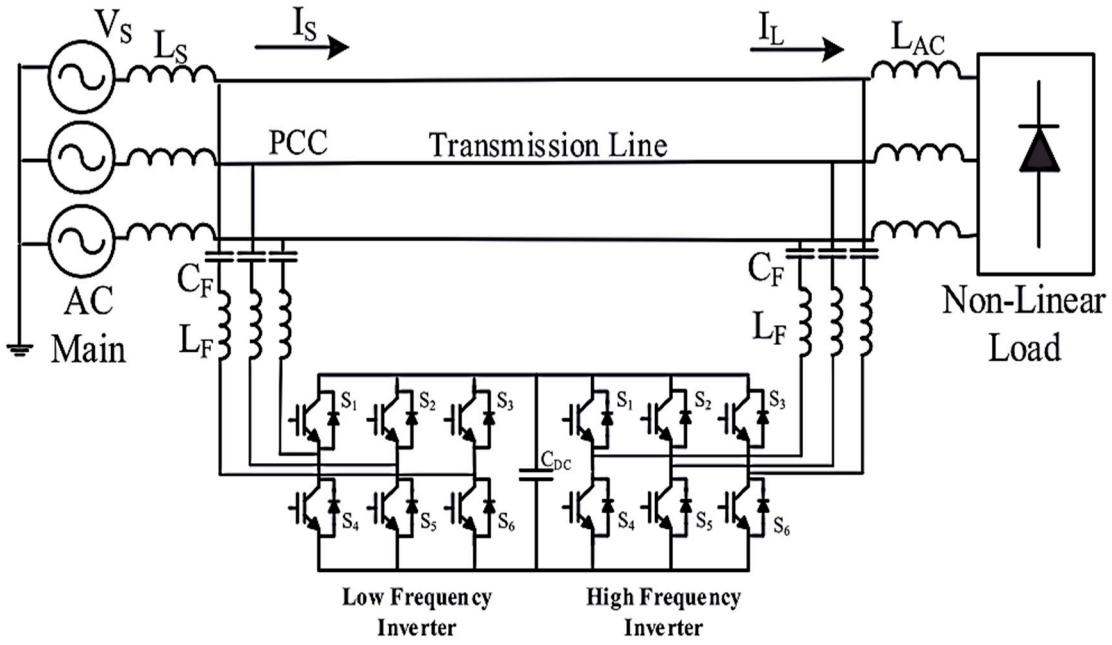

Figure 6. APF circuit with twelve switches in parallel [102].

4.3. Four-Wire, Three-Phase APFs

The ubiquitous six-switch, three-phase inverter [103] is utilized for standard-mode space voltage monitoring and comparison. One of the many features of a three-phase, four-wire device is a neutral current. Reactive power, current load, and an unbalanced current are additional factors. The current findings show that the negative and no sequence components produce the greatest results. In three different configurations—split condenser (2C), four-leg (4L), and three bridges (3HB) of nonlinear load—it is intended to handle a range of power output challenges [104]. The split condenser (2C), four-leg (4L), and three bridges H (3HB) of nonlinear load are three different configurations in which the three-phase, four-wire (3P4w) SA PFT is intended to manage a variety of power output challenges. A rectifier and an inverter, for a total of eight DC connections, are present in each of the six switches' [105]. A zigzag transformer and a zero series are used in the four-wire APF

technique to lessen the negative effects. The inverter-interlaid method is advised when determining the trigger impact of power transfer, nonlinear loads, asymmetrical loads, and power [106]. Specifically speaking, the DC-Link Condenser Switching losses in two-level inverters are smaller than in loose, interleaved inverters. The bearing current, shaft voltage, and early motor loss were eliminated along with the common-mode voltage variation using a DC voltage management system and a CMV removal system. Organizational limitations force a trade-off between switching ribbons and pre-existing errors in the semi-bridged transition system. Change and dead time distortion becomes more apparent as the switching frequency is increased. In order to minimize output current and transition, the ZVS converter uses a gentle switching approach such as the three-level diode constrained by two condensers, and a three-level DC/DC circuit is created to handle the voltages of the two input condensers.

5. Inverter Topology for Back-to-Back Inverters

The topology of the inverter in three phases is presented in Figure 7. Both inverters are reverse-linked to the common DC-link condenser. Its key benefit is that it enhances the capacity of the APF to compensate.

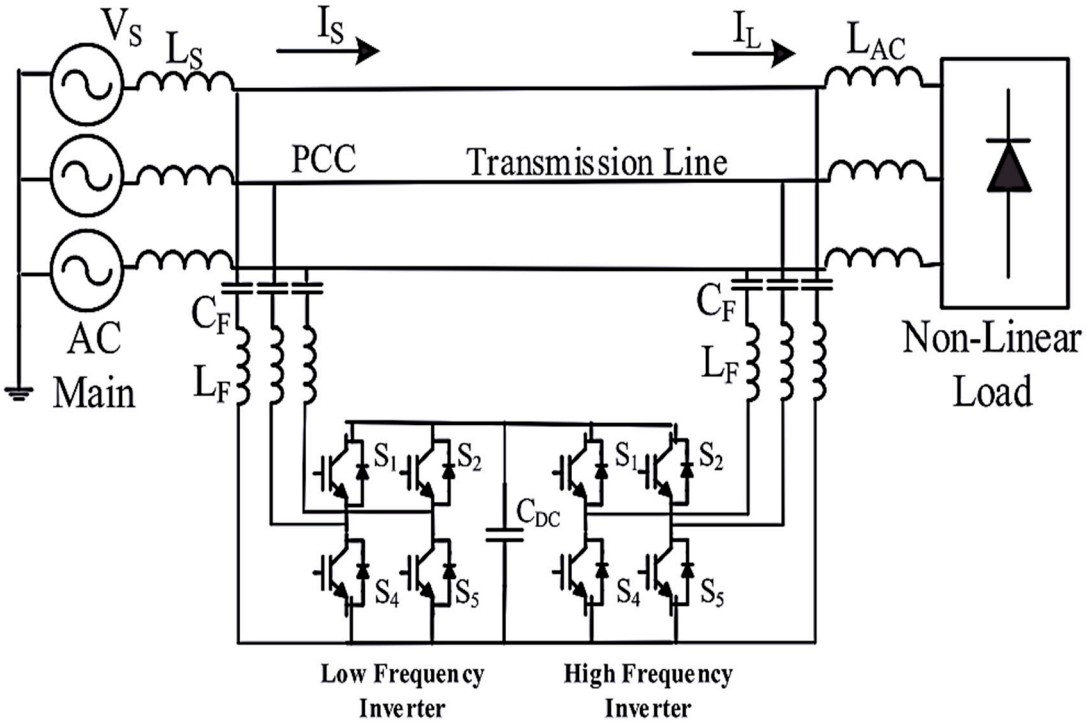

Figure 7. APF circuit with eight switches in parallel [106].

5.1. APFs with Two Wires (Single Phase)

The two full-bridge inverters function similarly to the six-legged dual switches for two single-stage nonlinear loadings. The output circuit is a single converter and has the highest output pressure without a corresponding transformer. A solution for transforming a single-phase system into a three-phase system is a reduced-switch account—universal APF [107]. A power loss causes a transient time delay in a half-bridge USPS configuration [108]. To prevent transitions, an offline UPS system with a standard transformer is installed on a simple winding sequence. In regular mode, it acts as an active filter, and in backup mode, it acts as a battery standby loading [109]. Table 5 compares three different configurations of the back-to-back inverter, depending on the number of switches removed. The UPS half-bridge design, which was simplified by the eight switches, used a four-switch transformer and a four-switch inverter. Because of the standard input and output neutral materials, it

also removes the insulation transformer [110]. Unlike traditional UPS systems, the number of interrupters and static switches is limited.

Table 5. Topologies of common-leg inverters with reduced switch counts.

Schemes/Methodology	References			
	[80]	[83]	[90]	[97]
Methodology	Four arm, Five arm	Four arm	Six arm	Three
Capacity (kVA)	1.5	1.5	2.5	2
Switching frequency (kHz)	5	3	6	12
Reduced switch count	4, 6, 7	8	4	6
Grid voltage (V)	100	110	220	210
THD %	3.5	1.6	1.9	2.3
Probable Efficiency	Medium	Low	Medium	High
DC linked voltage (V)	100	210	230	250

5.2. APFs with Three Phases (Wires)

A double HAPF inverter topology, as shown in Figure 7, consists of two back-to-back power converters sharing a DC-link condenser. Switching operations make use of information and input management. Large condensers and high DC bus pressures are needed in high dynamic load systems in order to maintain a larger stability margin and reduce stress on any condenser. On the DC link condenser, a topology of the split condenser (B4) with a low cost and marginal voltage constraint is used [111]. The third component is connected to the split capacitor legs' neutral mid-point, reducing the 12-switch power converter to an eight-switch power converter. The negative pole of the DC connection [112] is connected to the third level, which is ideally reduced in topology by a restriction of the split condenser topology. It improves process performance, reduces costs, and retains low voltage in the DC condenser even though the construction of hardware and controllers is very difficult. The LC PF was tuned to 550 Hz, after further testing, so that the lower-order harmonics were mitigated and a DC-link voltage was maintained. With a frequency of 750 kHz, the LC PF is tuned to high-degree harmonics. Both orders deal with harmonic mitigation in a complex and cogent manner. In each bridge inverter, a dual, four-button reduced count is suggested, as opposed to the standard twelve-button double-bridge inverter [113]. Load balancing and frequency exchange are done with and without redundancy in the two filters to maximize harmonic compensation and keep the grid stable. Separate DC condensers or transformers are used to block the zero-series current that circulates between the inverters. To connect three or two-leg series-parallel power translators, the line-interactive topology [114] is used. The three-phase, unidirectional, seven-phase resonance inverter is linked to three other command-line switches to achieve bidirectional power flow [115]. The neutral terminal is connected with the negative end of the DC condenser during a three-phase APF (four wires) [116]. The proposed UPQC architecture with neutral clusters reduces source current, the number of modules, DC-link voltage, switching frequency, and THD. To control each limb independently, shunt and series inverters require a capacitor-voltage balance, which increases the size and cost of the system. The system can be kept as compact as possible with a three-stage voltage regulator, synchronized compensation devices, and a T-connected transformer (Scott-Transformer) [117]. The DC-link voltage of the APF device is regulated by a normal condenser and the inductor by additional condensers in order.

5.3. Three-Phase (Four-Wire) APFs

The neutral terminal of the DC capacitor is connected to the negative end of the UPQC unit [118] to minimize the overall size of the UPQC unit. The suggested neutral-clamped UPQC configuration has a lower DC-link voltage, an average switching frequency, and less total harmonic distortion (THD) in the source current. Shunt and series inverters must include capacitor voltage balancing so that the devices may run each leg independently,

which increases the size and cost of the equipment. To keep the device as small as possible, a three-phase voltage source converter with distributed static synchronizers and a Scott-T transformer with a t-connection are all included in the design. Additional condensers are connected in series with a condenser and an inductor to increase the DC-link voltage of the APF system.

5.4. Common-Leg Inverter Methodology

An inverter with three phases and a common leg is arranged in a back-to-back arrangement. An APF correction device and an inverter are linked together via a simple DC-linking condenser, which may be utilized for single- or double-leg sharing [119]. Leg switches, which are commonly used in corrective and inverter operations, are typically activated. Single phase (two-wire) and three phases (three wire) are covered in the following sections (three wire).

5.5. Single-Leg APFs

Single-leg inverters' sharing is used to create two DC-link five- and six-leg configurations, along with a single-step, two-wire APF system. It has an inductor and a DC connection condensing system [120] to reduce the component count of the unit. As normal APF for current harmonic compensation, a reciprocal connection between the half-bridge and fully-bridge inverters is used. The power function is tracked by a parallel series injection transformer [121]. The topologies of the three common-leg H-bridges are compared in Table 5. The six-arm bridge voltage regulator is limited to the switching equipment by low-cost AC condensers. The origins and load of a single-phase, three-leg converter share one leg [122]. A three-leg converter with six switches is upgraded to a four-leg converter with four switches. Bidirectional power transfer, unit power factor, and sinusoidal input current regulation has been studied [123]. One leg of a three-legged converter in one stage shares the source and load. A three-legged six-switch converter is turned into a two-legged structure of four switches. A single-phase UPS system is strong, effective, and easy to manage voltage fluctuations [124]. The first leg of this rectifier nonlinear loads the battery bank; the middle leg sets the line frequency; and the third leg regulates the output voltage [125]. The general leg uses minimized power losses, low-cost design, and reactive energy control to reduce the number of switches.

5.6. Three-Leg APFs

The circuits for the rectifying and converting systems share the middle leg of a three-leg converter circuit with nine switches [126]. The middle switches supply input and output power. In two fixed and variable frequency modes, a virtual DC drive mechanism provides unit power factor, waveform input, and waveform output, a double-switch converter seeks, compared to the eighteen-switch converter matrix, to cut output costs. Due to the excessive weight of the DC-Link condenser that switches over-pressed semiconductors, the same speed is created by nine switch-on converters. In addition, it is necessary that the switching ratings of IGBT systems be increased and losses higher than in-back 12-switch converters, along with the downgraded amplitude and phase change in the terminal exit [127]. There are two auxiliary switches to increase DC–DC converter performance, including a single auxiliary switch. A soft switching technique with heavy switching loss and electro-magnetic interference allows the passage of zero voltage and zero current [128]. With the AC engine drive mechanism, several legs and loads are shared within the grid in one to three phases. In a four-leg setup, they are limited to eight switches. Since they share a single leg, a lower configuration of the switch is used instead of tenswitch configurations [129]. The sharing of the same results in cheaper output for various four-, five-, and six-legged conversions with regulated gate drives, diodes, and fuel. It increases unit defects, fault tolerance, installation size, process, and condenser current values through an increase in standard current and a decrease in DC voltage [130]. To minimize the size of passive components, two voltage-sourcing APFs are connected to the power line by means of standard mode coils and a DC

condenser. A standard stage-leg procedure is used, without using passive materials in any converter, to minimize device size and costs. The controller is designed to use space vector modulation and high-bandwidth control to prevent a passive LC filter from being replaced with a power filter [131].

6. Classification of Variable by Compensation

Active filters have been designed to improve certain power system features. These characteristics lead to the divisions described in Figure 8 that are included in the following section of the controlled system parameters.

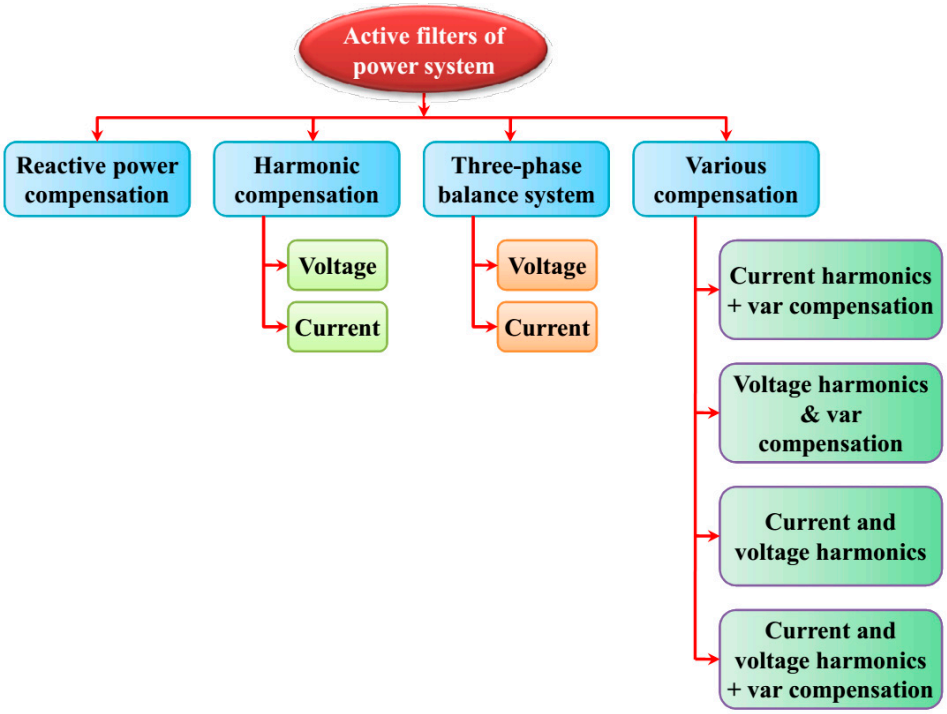

Figure 8. Classification by compensation.

6.1. Compensation for Reactive Power

Power compensation is quite popular in combination with current harmonics and numerous publications are discussed. On the other hand, active filter configuration does seldom address the problem of power factor correction by itself, since the market also has other quasi-dynamic reactive power countervails, which are cheaper and slower. Using this technique (in this case, reactive power filtration) as the currents needed to offset reactive power are of the same size as that of the rated load current, it would normally be suitable for applications with low power. In some cases, the management of sophisticated equipment would be a waste of single-phase systems where accurate compensation without producing harmonics is required without the use of additional power corrector devices, such as thyristor-driven reactors and condensers [132,133].

6.2. Harmonic Compensation

The compensation technique in power systems is the voltage-harmonic compensation separated into voltage- and current-harmonic compensation [134] which is the most important characteristic.

6.3. Compensation for Harmonic Voltage

The consumer-point terminal voltage, the point of common connecting (PCC) is typically within the slow and completes standard voltage range and is not significantly different from the load. For sensitive, harmonic voltage [135–138] devices, such as power

system protection devices and magnetic energy storage for superconductors, which require a purely sinusoidal supply, this problem is normally important [139–144]. When PCC harmonics are reduced, current harmonics are reduced significantly. Even though harmonic voltage compensation on the PCC eliminates the need for current harmonic compensation with nonlinear loads, it does not eliminate the necessity for current harmonic compensation [145].

6.4. Compensation of Harmonics Current

In low and medium-power applications, current harmonics are significantly balanced. The adjustment of current harmonics decreases voltage distortion greatly at the point of common coupling as indicated before. Many of the system design criteria depend on the actual size and configuration of loads. The RMS value of the overall current (for cable reduction and feeder losses) is always recommended since it signifies a reduction in current harmonics. Harmonic rules will soon compel manufacturers and installations to inject the number into the power grid [30,31].

7. A Three-Phase Balance System

Since currents and hence voltages are not balanced in these three phases and spaced 120° apart in time, in low- and medium voltage systems this is a major problem.

7.1. Network Voltage Balance in Three-Phase Systems

The scale of the imbalance of the system depends on the extent and scale of the current imbalances. This might lead to the uneven magnitude and unequal time intervals in the three-phase voltages. This is owing to the high impedance in supply. To obtain every phase of the sinusoidal reference form apply the required voltage for every phase. In such cases, the system performance of medium and high-powered systems, usually in the low power class, does not have any significant impact [146].

7.2. Current Balances in Three-Phase Systems

This compensation applies mainly to three-phase low power systems as regards balance voltages. Because in distribution systems with a low voltage for residential loads, the magnitude of the current delivered into the grid depends mostly on the imbalance level in the system [147]. The compensating system sometimes requires that the current value is delivered and limits its capacity to handle energy. The power system usually consists of three phases, each having its electricity storage component (H-bridge inverters).

7.3. Various Compensation Schemes

To improve filter efficiency, the above systems can be employed in various combinations. The following are the most popular combinations.

7.4. Reactive Power Compensation in Harmonic Currents

The most popular technique and harmonic filter are used to mitigate the harmonics and voltage of the feeder current. This technology has several advantages over other options, with only one filter required to make it all the better than many different types of countervailing equipment. Though due to the limitations imposed by the power switching ratings, this application can only be used for low-power applications. For more powerful applications that limit the filter to low power, the resulting switching frequency would have to be lower [148].

7.5. Reactive Power Compensating Harmonic Voltages

This combination, though uncommon, takes place in certain voltage harmonics configurations that normally affect the reactive power compensation indirectly. This compensation is suitable only for low-power applications.

7.6. Currents and Voltages Harmonic

A series-parallel combination of active filtration settings is possible to deal with the problem of simultaneous management of harmonic currents and voltages. This is very important and useful to ensure harmonic effects are free for supply as well as for load. However, this configuration is complex and normally reserved for very sensitive technologies such as electrical systems and magnetic storage systems.

7.7. Harmonic and Reactive Power Compensation

It manages reactive power and harmony, making it the latest system. This technique requires a concurrent succession of active filter setups Figure 9. Due to the difficulty of monitoring and lack of information in the literature, this is often rarely utilized.

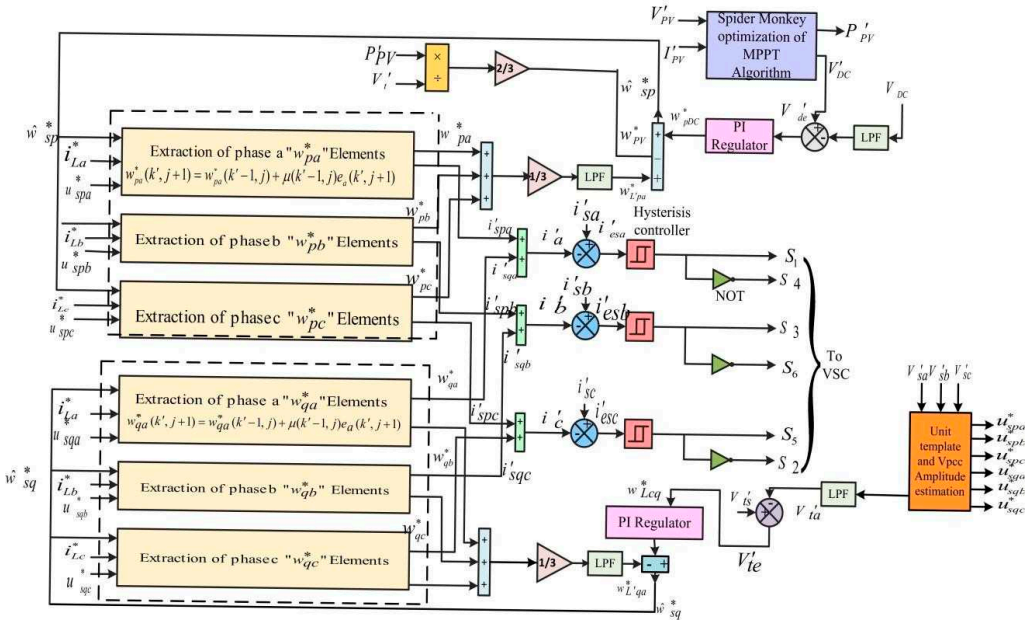

Figure 9. Scheme for reactive power compensation in GCPVS [59].

8. Classification According to Control Technology

Control techniques currently available are classified in different methods as in Figure 10. The techniques are classified mainly into open- and closed-loop control algorithms. As indicated in Figure 10, the closing loop controls are divided into other technology.

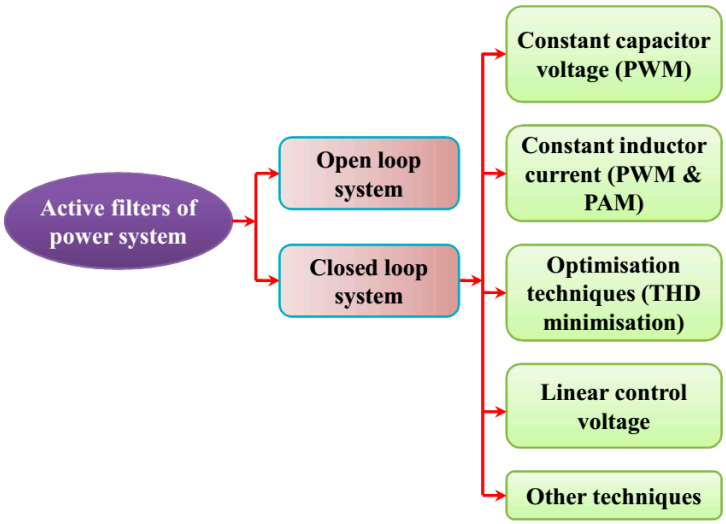

Figure 10. Classification of control techniques.

8.1. Open-Loop Control Systems

Open-loop systems consider load current and harmonics. They compare the most harmonic and/or reactive forces to the system as a current using a predetermined power level. There were several traditional filtering methods as third harmonic injection removal, the provisions of equipment for harmonic cancellation [2], and, standard pattern of load harmonics.

8.2. Closed-Loop Control Systems

The closed-circuit procedures contain a feedback loop that considers the required variables, in contrast, to open circuit systems. These systems are more precise from a harmonic and reactive power reduction perspective. These controllers generally use digital signals (DSPs). The control circuit should not be confused with the commonly used internal hysteresis systems, which are now standard blocks in most power-regulated inverters.

8.3. Scheme of Constant-Capacitor-Voltage

This method can be used in a DC connection with a condenser for single-stage or three-stage inverters. Depending on how the condenser voltage is connected to the power source, it may be possible to control the wave's shape. This is done by connecting the condenser to an inductive smoothing device. A standardized system for managing PWM technology results from this. The power source or the removed condenser changes the voltage across its ends. It is decided to keep this voltage within certain bounds by using a reference voltage. The discrepancy between the condenser value and the actual voltage serves as the basis for calculating the active force component for filter loss. This error differential is employed in conjunction with the current control error signal to establish the overall system failure that the controller has been processing. This tactic is very well-liked, as shown by numerous references [149].

8.4. Scheme of Constant-Inductor-Current

This control mechanism is suitable for ordinary converters connected to the inductor in a DC connection. When the condensing voltage is substituted with the inductor current, it works very much like the operation of a constant condenser system voltage. This approach is carried out using two major methods:

i. Modulation of current pulse-width: the PWM controls supply pulses, such asin the case of the continuous condenser voltage, to represent the medium signal at a given period.
ii. Modulation of current pulse-amplitude: active filters are available to modulate the current wavelength needed under the new method for controlling [52]. Although the concept is well established, the current power technology cannot be implemented.

8.5. Optimization Techniques

The optimization procedure is the same for switched condensers and gate filters. The capacitor size and starting voltage are the most important factors in determining the pace of current and amplitude growth. These elements are the functions of the pattern and offer considerable flexibility to the waveform of the current drawn by the filter. For the switches, it is necessary to determine the correct switching function. In addition to minimizing THD or the fundamental component of the filter current a set of different load current harmonics is the main focus of the system control. There is a delay in the time when a fresh set of switching angles generated from the optimizing technique is the detection of a harmonic current change and application [150–154].

8.6. Linear-Voltage-Control Technique

The detection of harmonic current takes time and the use of new switching angles obtained through the optimization process is delayed. This system is particularly suited for

slowly varying or varying loads. The smooth condenser voltage change, on the contrary, guarantees that the supply/filter loop monitors current variations, which lowers the change frequency further. This technique has the advantage that the supply side does not change the sudden voltage, which reduces the amount that the PWM inverter presents of high-frequency harmonics [146].

8.7. Intelligent Control Schemes

8.7.1. Fuzzy Control

Using if–then rules, a fuzzy logic controller might present a control protocol as "If the temperature is low, open the heating valve slightly" [110]. Figure 11 illustrates the use of fuzzy sets, which are sets with overlapping borders, to express the ambiguity (uncertainty) in the definition of linguistic concepts. Because of the fuzzy set structure, a given domain element can belong to numerous sets, each of which has a different level of membership.

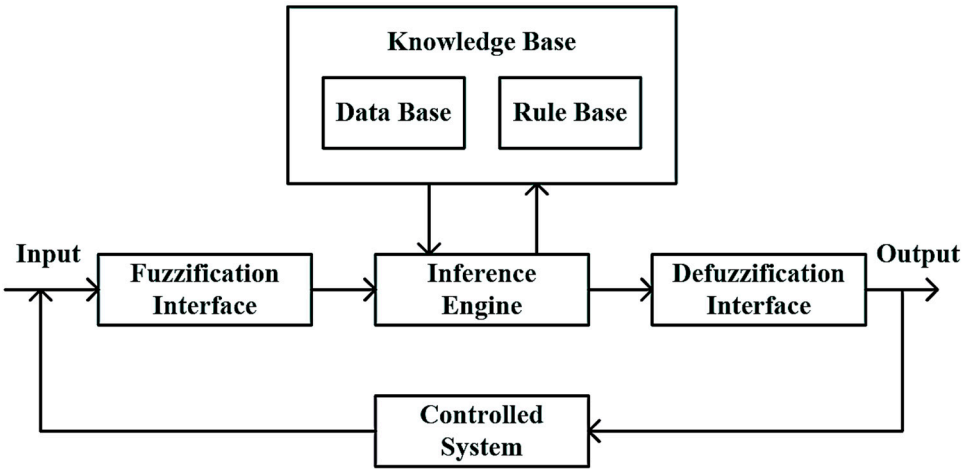

Figure 11. Fuzzy control techniques [110].

8.7.2. Artificial Neural Network Control

An LCL-filter based single-phase solar inverter vector control method is the primary task of this project's ANN component development. Using approximation dynamic programming, as shown in Figure 12, the ANN controller is trained to achieve optimal control performance. On one hand, it is used to assess how well an ANN-based renewable energy system performs by modeling the PV system's grid integration and maximum power extraction and then creating an experimental solar PV system for hardware validation [118]. In both simulation and hardware implementation, the ANN control outperforms the usual standard vector control technique and proportional resonant control approach in terms of performance.

8.7.3. Neuro-Fuzzy Control

The parameters of a neuro-fuzzy system (fuzzy sets and fuzzy rules) are determined by processing data samples in a learning algorithm developed from or influenced by neural network theory [125]. One way to make the most of PV systems is to use an active power line conditioner, such as the one shown in Figure 13, which is intended to balance the nonlinear and unbalanced loads of PV systems. DC–DC and DC–AC power converters are needed for the grid integration of PV systems to optimize the generated PV power and to inject AC current into the network. As part of this research, a neuro-fuzzy system and a fuzzy logic control loop are built to ensure that the PV system connected to the DC side is always operating at its maximum power point (MPP). Nonlinear and unbalanced loads in the electrical system are actively compensated for in the DC–AC power converter management approach.

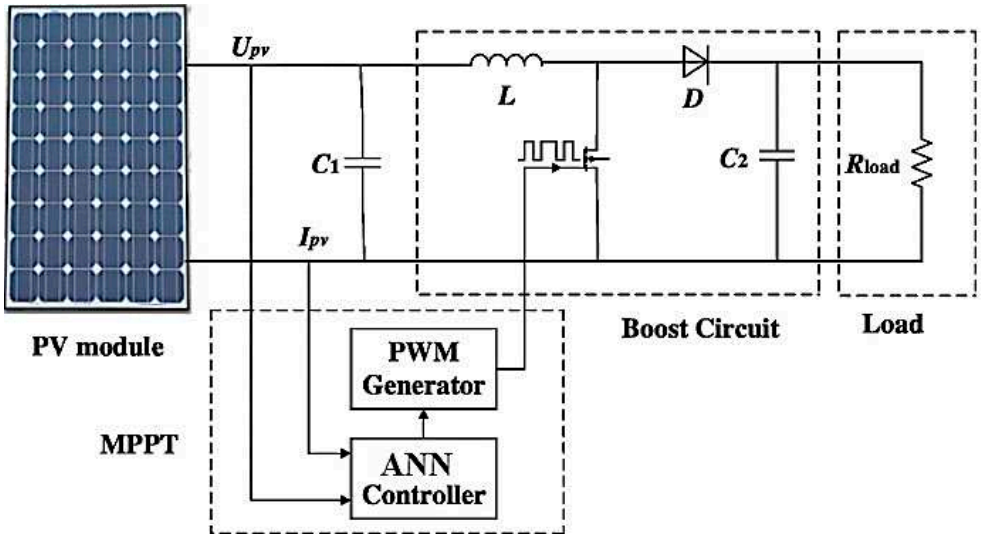

Figure 12. Artificial neural network control techniques [118].

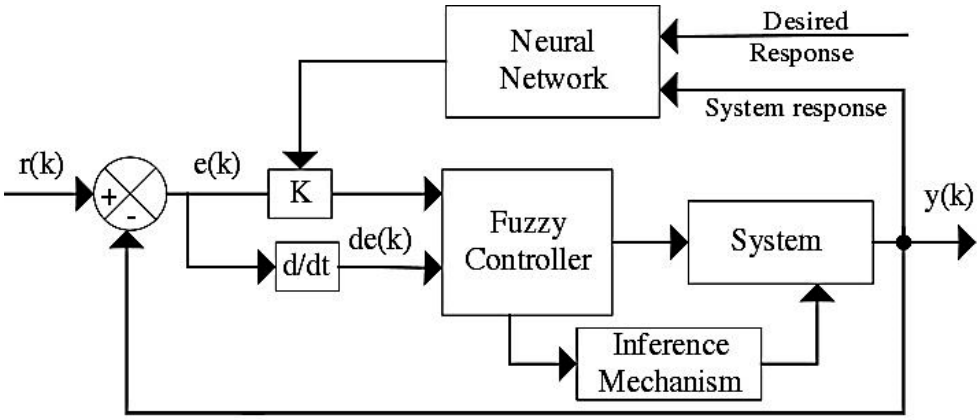

Figure 13. Artificial neural network control techniques [125].

8.7.4. Adaptive Neuro-Fuzzy Inference System (ANFIS) Controller

ANFIS, or the Adaptive Neuro-Fuzzy Inference System, is a powerful new approach to research that integrates fuzzy logic and artificial neural networks. The design of ANFIS controller in the face of diverse disturbances is presented here [67,108]. Another key consideration is the LC filter's stability, which is meant to reduce unwanted harmonics. Faster dynamic performance has been achieved.

8.8. Robust Control Schemes

8.8.1. H infinity Controller

The use of H infinity control synthesis has been proven to ensure robustness and high performance. A high level of disturbance rejection ensures that the system remains stable under all operating conditions. Designs for H infinity controllers may make use of any number of methodologies, but because performance weights may be introduced during design, H infinity loop shaping is particularly popular. This is a mixture of weighted closed-loop responses from the H Infinity controller (Figure 14) [148], based on design criteria such as model uncertainty and disturbance attenuation for higher frequencies, as well as the closed-loop plant's bandwidth requirements. A great deal of control effort is required while using H-Infinity controllers because they are so powerful. It is also possible that the design may be dependent on a certain system and will thus need an in-depth examination of that system. Using the H-optimal technique, extra frequency-dependent

weights are included in a plant to display certain stability and performance characteristics relevant to the design purpose stated at the outset.

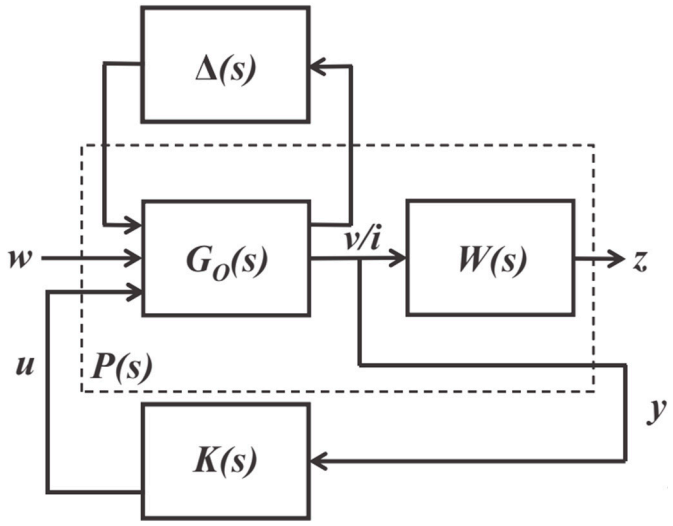

Figure 14. H∞-optimal control techniques [148].

8.8.2. Sliding Mode Control (SMC)

SMC is a nonlinear control method distinguished by its high degree of precision, resilience, and simplicity in tuning and implementation. To put it another way, SMC systems are intended to push system states onto a certain area of state space known as the "sliding surface."PV power system efficiency may be improved by using this controller instead of taking atmospheric variables into account to ensure optimal MPP operation (Figure 15) [95,149]. As a result of our suggested controller, the power oscillation around the operating point is eliminated. The suggested controller has an adaptive SMC gain that may be used to compensate for the unpredictability of the surrounding environment.

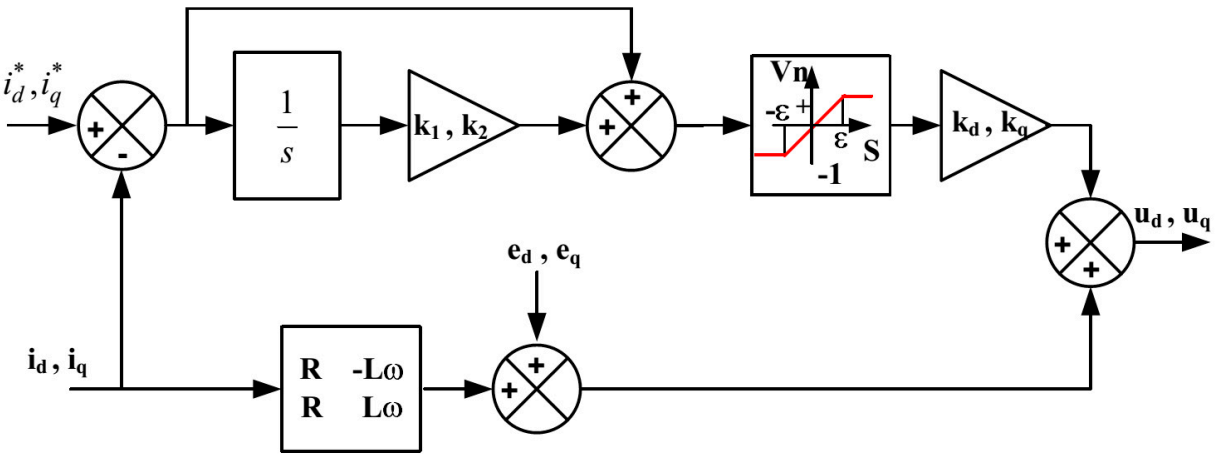

Figure 15. Sliding mode control techniques [149].

8.9. Optimal/Predictive Controllers

8.9.1. Predictive Dead-Beat Control

In the theory of discrete time control, this method is employed. The "dead-beat control issue" in discrete-time control theory refers to determining the input signal that must be supplied to a system for the output to reach a steady state in the fewest number of time steps. Many process control systems employ deadbeat controllers because of their dynamic features. Classic feedback controls are used to set control gains in PV systems, and these

are determined by referring to a table based on plant system order and normalized natural frequency [92,93].

8.9.2. Linear Quadratic Regulator

One of the most widely used design techniques is the linear quadratic regulator (LQR). Figure 16 depicts a maximum power point tracking method based on a linear quadratic regulator (LQR) for a standalone photovoltaic system [150]. The advantages of the method are faster tracking ability, the transfer of maximum deliverable power, and its implementation with reduced complexity.

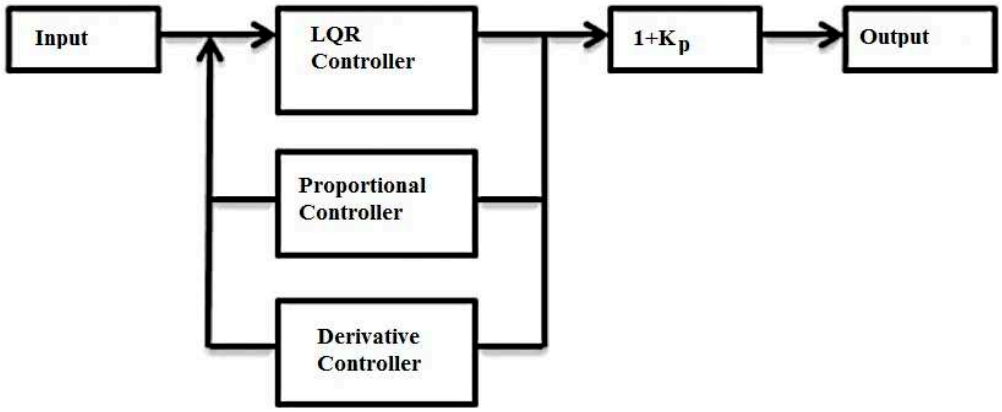

Figure 16. Linear Quadratic Regulator control technique [150].

8.10. Predictive Control

The PV array in Figure 17 is controlled using the model predictive control (MPC) approach [93,151] to get the most electricity out of it and send it to the grid. To make the PV system economically viable, the stochastic nature of solar energy needs the use of MPPT.

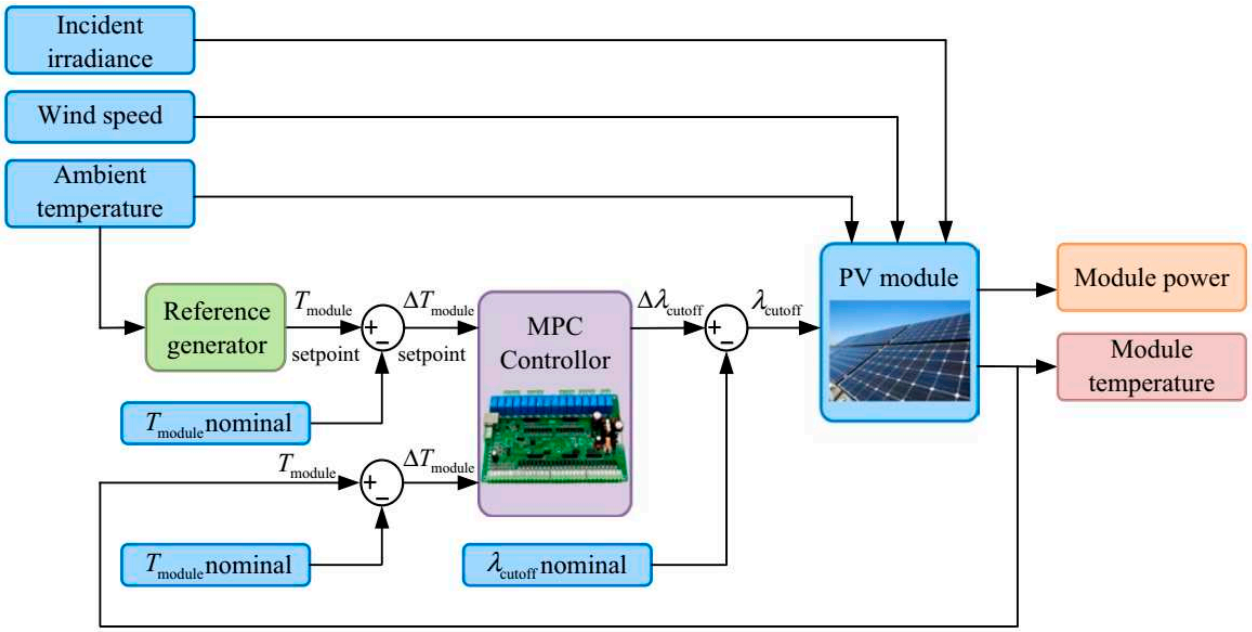

Figure 17. Predictive dead beat control techniques [151].

8.11. Other Techniques

More options are available for control. They modify the above-mentioned technologies to produce new or better performance compared with their predecessors shown in Table 6. That may mean modern adaptive, predictive, and sliding controls which, without the

help of DSPs, are difficult to obtain. These algorithms operate in the time and frequency fields [148].

Table 6. Topologies of Common-Control Topology are Compared.

Schemes/Methodology	References			
	[125]	[110]	[149]	[148]
Methodology	ANFIS	FUZZY	SMC	H∞
Capacity (kVA)	2.2	2.3	1.6	1.2
Switching frequency (kHz)	5	3	6	12
Reduced switch count	4, 6, 7	8	4	6
Grid voltage (V)	110	220	240	210
THD %	1.8	2.2	1.9	2.3
Probable Efficiency	Medium	Low	Medium	High
DC linked voltage (V)	100	230	230	220
Complexity Level	High	High	Medium	Low
Application	Grid	Stand-alone	Stand-alone	Grid
Parameter Tuning	Yes	Yes	Yes	Yes
Converter Type	DC/AC	DC/DC	DC/AC	DC/AC
Commercial Application	Vacuum gas oil hydrocracking plant	Facial pattern recognition, air conditioners, washing machines, vacuum cleaners	Electric drives, robotics	Commercial satellite, robust control

9. Discussion and Analysis

9.1. Reduced-Switch-Count Inverters

a. The differences between the reduced transformer-less and the reduced transformer-grid-related inverter topologies are summarized in Table 6, which can be found here. To create considerable amplitudes of alternating current voltage in a back-to-back architecture, a much bigger DC connecting condenser and a significantly higher DC voltage is necessary. Because of the high voltage, it is difficult to overdress the buttons on the semiconductor. To tackle this problem, a z-source network and a modulator interruptive system [75] are used. On the other hand, for the B8 converter, eight switches are employed, and there is a shared DC connector [76]. When both systems are up and running and in sync at the same time, the DC connection does not transport any vital data streams between them. To get around the B8 converter restriction, a five-leg converter is used to exchange the fifth-phase beam between the two converters [134]. Because the usual frequency imposition between two AC interface conditioning machines, including series shunt drives and DC-settling drives, does not significantly differ in tension, the normal frequency imposition between them is limited. SAPF has lately gained prominence as a tool for improving power efficiency in networked and renewable energy conversion systems. In recent years, both classic and sophisticated techniques and capacity controls, harmonic lowering, and dynamic reactive power compensation, as well as supplementary functions, have been investigated. Table 6 presents a summary of the findings and parameters derived from the APF topologies that were recently discussed in Section 4. For each topology, the most cost-efficient, effective, and appropriate architectures are identified and tested. The findings of this research are as follows:

b. The traditional back-to-back power converters restrict the use of a DC-Link condenser, reduced amplitude shares, and unregulated phase transmission at the output terminals between the two converters.

c. The back-to-back topology allows for individual adaptation of both converters while they are disconnected. It is constrained by the low modulation ratio, which, despite the topological function, creates calculative difficulties [135].

d. While this is based on the number of switches used, lowering the number of switches improves overall reliability and decreases dissipated conduction and switching errors.

High voltage and current tension are applied to both switching components in a high-power rating device, influencing the inverter's performance.

e. The two terminal sets have a limited phase change and a strict sharing of amplitude with the AC–AC topologies such as the two motor drives [136], inverter-rectifiers and UPS [138].

f. The output terminals are set for the same output voltages by replacing the carrier with two converters, doubling the DC connection voltage, and doubling the semiconductor voltage. This doubling effect is avoided by using lower switch counting topologies.

The efficiency comparisons of the three topologies in reduction counts are described in Tables 4–6. The number of switches that are reduced, stability, part ratings, and THD are all factors that are considered. Inverter switches have a modest level of efficiency, according to studies [96,97]. Three switches had the best average performance (94–96%) [95], despite having highly rated modules. The DC-voltage link's rating and condenser dimension have a significant impact on the number of switches and inverter legs needed. The conventional topology of the inverter is distributed among the converter legs with a low DC connecting voltage, especially in comparison with the reduced topology of the switch counting [96]. A serial combination of condensers helps reduce DC speeds, which leads to more active and passive components and a higher unit cost [98]. This reduces the power of having fewer switches.

9.2. PV Inverter Linked with a Grid

The high cost of inverters and the numerous components needed can be offset by the system's dependability and performance when combined with some PV grid interactive solutions. This connects the power grids to transformer-free, multilevel, multiple-function inverters that are centralized on the APF when used in PV and WECS. Grid-connected PV inverters without transformers are a great way to lower grid-connected system costs while also reducing the size and weight of the grid-connected system. No galvanic insulation is needed because there is not a transformer [137], which leads to increased induced leakage strength, a less effective overall voltage mode (such as output defects and protection issues), and safety hazards. The transformer-less inverter H5 [140] must have high effectiveness [142] and leakage current suppression in order to operate properly due to its design. The junction capacity of the switches accounts for the leakage current's continued high level during the freewheeling mode. However, problems involving voltage fluctuation are approached from two different angles. Solar PV panels are initially cut off from the power grid while engaging in unrestrained activities. The PV plate is then connected to a cable at one end. Cascaded H-bridge topology's [32] ability to boost the voltage from an alternating current side output at the expense of a colossal amount of switching devices is one of its most appealing features. High efficiency and reliability (HERIC) [143] and H5 inverters are an additional choice. These inverters are especially well-suited for semi-bridge topologies and other applications. Since the neutral point is located in the middle of the input voltage, the gate signals must be synchronized. The transformer-free PV inverter does this by preventing leakage current while still maintaining a constant normal mode voltage using a circuit made up of six switches and two diodes. Better multi-level inverter topologies are currently used instead of traditional topologies to prevent leakage.

9.3. Recommendations

- To reduce harmonics and improve energy quality in transmission systems, some reports claim that grid-connected inverter circuit topologies and SAPF circuit methods have been recommended.
- Linear and nonlinear load mode operations will be recommended.
- Cost-efficient, effective, and appropriate architectures need to be recommended.

10. Conclusions

In the energy consuming sector, there is an increasing quantity of renewable energy equipment and linear and nonlinear loads such as nonlinear SVCs. These devices have an impact on everyday existence. Due to the replacement of a transformer, many issues arise, including output loss, security concerns, leakage current, and resonance circuit extension. The numerous configurations of power converters as an interface between energy providers and renewable energy can then be exchanged based on their topological structure and modulation scheme. A fault between voltage modes and the absence of leakage flux in a grid structure caused an increase in voltage and frequency compared to conventional topologies. This review article provides a classification of available techniques for use of active power filters based on the type of circuitry, topology, control variables involved, control algorithm, and compensation techniques to select an APF technique for application in grid connected renewable energy systems. This review is expected to be a helpful tool for designers, commercial manufacturers of grid-connected systems, and for APF users.

In the future, an idea about linear and nonlinear load mode operations and types of preferable inverters used will be discussed. The further review has also included balanced and unbalanced conditions. Additionally, the efficacy calculation process for the application of APF in grid-connected renewable energy systems will be discussed.

Author Contributions: Conceptualization, D.K.D. and P.K.S.; methodology, D.K.D. and P.K.S.; formal analysis, D.K.D. and P.K.S.; investigation, D.K.D. and P.K.S.; resources, D.K.D. and P.K.S.; writing—original draft preparation, D.K.D. and P.K.S.; writing—review and editing, D.K.D. and P.K.S.; Authors has reviewed and edited the draft. All authors have read and agreed to published version of manuscript.

Funding: This research received no external funding.

Data Availability Statement: This article has no associated data.

Conflicts of Interest: The authors declare no conflict of interest.

Abbreviations

PV	Photovoltaic
GCPVS	Grid connected PV system
APF	Active Power Filter
WT	Wind turbine
AC	Alternating Current
SAPF	Shunt active power filter
HAPF	Hybrid active power filter
MFI	Multifunctional Inverter
THD	Total harmonic distortion
WECS	Wind energy conversion system
PCC	Point of common coupling
PWM	Pulse width modulation
SDBR	Series Dynamic Braking Resistance
DBR	Dynamic Braking Resistance
SVC	Static VAR Compensator
STATCOM	Static Synchronous Compensator
TCSC	Thyristor Controlled Sequencing
OLTC	On Load Tap Changers
UPQC	Unified Power Quality Controller
CSI	Current source Inverter
VSI	Voltage Source Inverter
UPS	Uninterrupted Power Supply
IGBT	Insulated Gate Bipolar Transistor
MOSFET	Metal Oxide Semiconductor Field Effect Transistor
ZVS	Zero Voltage Switching

PF	Power Filter
ANN	Artificial Neural Network
MPPT	Maximum Power Point Tracking
ANFIS	Adaptive Network based Fuzzy Interface System
SMC	Sliding Mode Controller
LQR	Linear Quadratic Regulator
MPC	Model Predictive Control
V_s	Source Voltage
Is	Instantaneous source current
I_L	Instantaneous load current
I_c	Filter Current
V_{dc}	DClink Voltage
L_s	Source side inductor
L_{AC}	Load side inductor
C_F	Filter capacitor
L_F	Filter Inductor
C_{dc}	DClink Capacitor
L	Inductor
C_1	DC link Capacitor
C_2	Capacitor of Boost Circuit
D	Diode of Boost Circuit
r(k)	Control input
e(k)	Error
y(k)	Measured output
w	Noise
u	Control input
K(s)	Controller
W(s)	Weight function
Z	Controlled output
Y	Measured output
I_d	Active Current
I_q	Reactive Current
I_d*	Reference current
I_q*	Reference current
K_d	Constant
K_q	Constant

References

1. Wu, G.; Ruan, X.; Ye, Z. Non-isolated high step-up DC–DC converters adopting switched-capacitor cell. *IEEE Trans. Ind. Electron.* **2015**, *62*, 383–393. [CrossRef]
2. Liang, T.-J.; Lee, J.-H.; Chen, S.-M.; Chen, J.-F.; Yang, L.-S. Novel isolated high-step-up DC–DC converter with voltage lift. *IEEE Trans. Ind. Electron.* **2013**, *60*, 1483–1491. [CrossRef]
3. Sitbon, M.; Schacham, S.; Suntio, T.; Kuperman, A. Improved adaptive input voltage control of a solar array interfacing current mode controlled boost power stage. *Energy Convers. Manag.* **2015**, *98*, 369–375. [CrossRef]
4. Lotfy, M.E.; Senjyu, T.; Farahat, M.A.; Abdel-Gawad, A.F.; Yona, A. Enhancement of a small power system performance using multi-objective optimization. *IEEE Access* **2017**, *5*, 6212–6224. [CrossRef]
5. Cumulative Development of Various Renewable Energy System/Devices in Country. Available online: http://mnre.gov.in/mission-and-vision-2/achievements (accessed on 30 April 2017).
6. Pathan, N.T.; Adhau, S.P.; Adhau, P.G.; Sable, M. MPPT for grid connected hybrid wind driven PMSG-solar PV power generation system with single stage converter. *J. Elect. Power Syst. Eng.* **2017**, *3*, 41–59.
7. Li, S.; Li, J. Output predictor-based active disturbance rejection control for a wind energy conversion system with PMSG. *IEEE Access* **2017**, *5*, 5205–5214. [CrossRef]
8. Fathabadi, H. Novel highly accurate universal maximum power point tracker for maximum power extraction from hybrid fuel cell/photovoltaic/wind power generation systems. *Energy* **2016**, *116*, 402–416. [CrossRef]
9. Fathabadi, H. Novel fast and high accuracy maximum power point tracking method for hybrid photovoltaic/fuel cell energy conversion systems. *Renew. Energy* **2017**, *106*, 232–242. [CrossRef]
10. Fathabadi, H. Novel high-efficient unified maximum power point tracking controller for hybrid fuel cell/wind systems. *Appl. Energy* **2016**, *183*, 1498–1510. [CrossRef]

11. Hong, C.M.; Chen, C.H. Intelligent control of a grid-connected wind-photovoltaic hybrid power systems. *Int. J. Elect. Power Energy Syst.* **2014**, *55*, 554–561. [CrossRef]
12. Baghdadi, F.; Mohammedi, K.; Diaf, S.; Behar, O. Feasibility study and energy conversion analysis of stand-alone hybrid renewable energy system. *Energy Convers. Manag.* **2015**, *105*, 471–479. [CrossRef]
13. Bhandari, B.; Poudel, S.R.; Lee, K.-T.; Ahn, S.-H. Mathematical modeling of hybrid renewable energy system: A review on small hydro- solar-wind power generation. *Int. J. Precis. Eng. Manuf. Green Technol.* **2014**, *1*, 157–173. [CrossRef]
14. Kwan, T.H.; Wu, X. Maximum power point tracking using a variable antecedent fuzzy logic controller. *Sol. Energy* **2016**, *137*, 189–200. [CrossRef]
15. Kabalci, E. Design and analysis of a hybrid renewable energy plant with solar and wind power. *Energy Convers. Manag.* **2013**, *72*, 51–59. [CrossRef]
16. Dihrab, S.S.; Sopian, K. Electricity generation of hybrid PV/wind systems in Iraq. *Renew. Energy* **2013**, *35*, 1303–1307. [CrossRef]
17. Kirubakaran, A.; Jain, S.; Nema, R.K. The PEM fuel cell system with DC/DC boost converter: Design, modeling and simulation. *Int. J. Recent Trends Eng.* **2009**, *1*, 157–161.
18. Nejabatkhah, F.; Danyali, S.; Hosseini, S.H.; Sabahi, M.; Niapour, S.M. Modeling and control of a new three-input DC–DC boost converter for hybrid PV/FC/battery power system. *IEEE Trans. Power Electron.* **2012**, *27*, 2309–2324. [CrossRef]
19. Revathi, B.S.; Prabhakar, M. Non-isolated high gain DC-DC converter topologies for PV applications—A comprehensive review. Renew. Sustain. *Energy Rev.* **2016**, *66*, 920–933.
20. Montuori, L.; Alcázar-Ortega, M.; Álvarez-Bel, C.; Domijan, A. Integration of renewable energy in microgrids coordinated with demand response resources: Economic evaluation of a biomass gasification plant by Homer Simulator. *Appl. Energy* **2014**, *132*, 15–22. [CrossRef]
21. Zhao, B.; Zhang, X.; Li, P.; Wang, K.; Xue, M.; Wang, C. Optimal sizing, operating strategy and operational experience of a stand-alone microgrid on Dongfushan Island. *Appl. Energy Jan.* **2014**, *113*, 1656–1666. [CrossRef]
22. Kuhn, V.; Klemeš, J.; Bulatov, I. MicroCHP: Overview of selected technologies, products and field test results. *Appl. Therm. Eng.* **2008**, *28*, 2039–2048. [CrossRef]
23. Patel, N.; Gupta, N.; Babu, B.C. Design, Development, and Implementation of Grid-Connected Solar Photovoltaic Power Conversion System. *Energy Sources Part A Recovery Util. Environ. Eff.* **2019**, *43*, 1–20. [CrossRef]
24. Ranaboldo, M.; Lega, B.D.; Ferrenbach, D.V.; Ferrer-Martí, L.; Moreno, R.P.; GarcíaVilloria, A. Renewable energy projects to electrify rural communities in Cape Verde. *Appl. Energy* **2014**, *118*, 280–291. [CrossRef]
25. Ma, T.; Yang, H.; Lu, L. A feasibility study of a stand-alone hybrid solar–wind– battery system for a remote island. *Appl. Energy* **2014**, *121*, 149–158. [CrossRef]
26. Deshmukh, M.K.; Deshmukh, S.S. Modeling of hybrid renewable energy systems. *Renew. Sustain. Energy Rev.* **2008**, *12*, 235–249. [CrossRef]
27. Natarajan, K.; Sankaramoorthy, M.; Rajkumar, A.; Shamshabad, T.; Kandlakoya, T. Controlling the Power Loss in Radial Distribution Network by Optimally Placing UPQC through Reconfiguration Using Evolutionary Algorithms. *Int. J. Pure Appl. Math.* **2018**, *118*, 161–179.
28. Calise, F.; Cipollina, A.; Dentice d'Accadia, M.; Piacentino, A. A novel renewable poly generation system for a small Mediterranean volcanic island for the combined production of energy and water: Dynamic simulation and economic assessment. *Appl. Energy* **2014**, *135*, 675–693. [CrossRef]
29. Chen, H.-C. Optimum capacity determination of stand-alone hybrid generation system considering cost and reliability. *Appl. Energy* **2013**, *103*, 155–164. [CrossRef]
30. Perera, A.T.D.; Attalage, R.A.; Perera, K.K.C.K.; Dassanayake, V.P.C. A hybrid tool to combine multi-objective optimization and multi-criterion decision making in designing standalone hybrid energy systems. *Appl. Energy* **2013**, *107*, 412–425. [CrossRef]
31. Perera, A.T.D.; Attalage, R.A.; Perera, K.K.C.K.; Dassanayake, V.P.C. Designing standalone hybrid energy systems minimizing initial investment, life cycle cost and pollutant emission. *Energy* **2013**, *54*, 220–230. [CrossRef]
32. Bhandari, B.; Lee, K.-T.; Lee, C.S.; Song, C.-K.; Maskey, R.K.; Ahn, S.-H. A novel off-grid hybrid power system comprised of solar photovoltaic, wind, and hydro energy sources. *Appl. Energy* **2014**, *133*, 236–242. [CrossRef]
33. Esmaeili, M.; Shayeghi, H.; Valipour, K.; Safari, A.; Sedaghati, F. Power quality improvement of multimicrogrid using improved custom power device called as distributed power condition controller. *Int. Trans. Electr. Energy Syst.* **2020**, *30*, e12259. [CrossRef]
34. Bekele, G.; Tadesse, G. Feasibility study of small Hydro/PV/Wind hybrid system for off-grid rural electrification in Ethiopia. *Appl. Energy* **2012**, *97*, 5–15. [CrossRef]
35. Bekele, G.; Palm, B. Feasibility study for a standalone solar–wind-based hybrid energy system for application in Ethiopia. *Appl. Energy* **2010**, *87*, 487–495. [CrossRef]
36. Rehman, S.; Mahbub Alam, M.; Meyer, J.P.; Al-Hadhrami, L.M. Feasibility study of a wind–pv–diesel hybrid power system for a village. *Renew. Energy* **2012**, *38*, 258–268. [CrossRef]
37. Fadaee, M.; Radzi, M.A.M. Multi-objective optimization of a stand-alone hybrid renewable energy system by using evolutionary algorithms: A review. *Renew. Sustain. Energy Rev.* **2012**, *16*, 3364–3369. [CrossRef]
38. Abbes, D.; Martinez, A.; Champenois, G. Life cycle cost, embodied energy and loss of power supply probability for the optimal design of hybrid power systems. *Math. Comput. Simul.* **2014**, *98*, 46–62. [CrossRef]

39. Hu, Y.; Solana, P. Optimization of a hybrid diesel-wind generation plant with operational options. *Renew. Energy* **2013**, *51*, 364–372. [CrossRef]
40. Kaldellis, J.K.; Kavadias, K.A.; Filios, A.E. A new computational algorithm for the calculation of maximum wind energy penetration in autonomous electrical generation systems. *Appl. Energy Jul.* **2009**, *86*, 1011–1023. [CrossRef]
41. Alsayed, M.; Cacciato, M.; Scarcella, G.; Scelba, G. Multicriteria optimal sizing of photovoltaic-wind turbine grid connected systems. *IEEE Trans. Energy Convers.* **2013**, *28*, 370–379. [CrossRef]
42. Ma, T.A.; Yang, H.; Lu, L.; Peng, J. Technical feasibility study on a standalone hybrid solar-wind system with pumped hydro storage for a remote island in Hong Kong. *Renew. Energy* **2014**, *69*, 7–15. [CrossRef]
43. Kapsali, M.; Anagnostopoulos, J.S.; Kaldellis, J.K. Wind powered pumped-hydro storage systems for remote islands: A complete sensitivity analysis based on economic perspectives. *Appl. Energy* **2012**, *99*, 430–444. [CrossRef]
44. Baquero, G.; Esteban, B.; Riba, J.-R.; Rius, A.; Puig, R. An evaluation of the life cycle cost of rapeseed oil as a straight vegetable oil fuel to replace petroleum diesel in agriculture. *Biomass Bioenergy* **2011**, *35*, 3687–3697. [CrossRef]
45. Saremi, S.; Mirjalili, S.; Lewis, A. Grasshopper optimization algorithm: Theory and application. *Adv. Eng. Softw.* **2017**, *105*, 30–47. [CrossRef]
46. Lakum, A.; Mahajan, V. Optimal placement and sizing of multiple active power filters in radial distribution system using grey wolf optimizer in presence of nonlinear distributed generation. *Electr. Power Syst. Res.* **2019**, *173*, 281–290. [CrossRef]
47. Moghbel, M.; Masoum, M.A.; Fereidouni, A.; Deilami, S. Optimal sizing, siting and operation of custom power devices with STATCOM and APLC functions for real-time reactive power and network voltage quality control of smart grid. *IEEE Trans. Smart Grid* **2017**, *9*, 5564–5575. [CrossRef]
48. Li, Y.; Feng, B.; Li, G.; Qi, J.; Zhao, D.; Mu, Y. Optimal distributed generation planning in active distribution networks considering integration of energy storage. *Appl. Energy* **2018**, *210*, 1073–1081. [CrossRef]
49. Sarker; Goswami, S. Optimal location of unified power quality conditioner in distribution system for power quality improvement. *Int. J. Electr. Power Energy Syst.* **2016**, *83*, 309–324. [CrossRef]
50. Lund, H. Renewable energy strategies for sustainable development. *Energy* **2007**, *32*, 912–919. [CrossRef]
51. Shahzad, M.K.; Zahid, A.; Rashid, T.; Rehan, M.A.; Ali, M.; Ahmad, M. Techno-economic feasibility analysis of a solar-biomass off grid system for the electrification of remote rural areas in Pakistan using HOMER software. *Renew. Energy* **2017**, *106*, 264–273. [CrossRef]
52. Sen, R.; Bhattacharyya, S.C. Off-grid electricity generation with renewable energy technologies inIndia: An application of HOMER. *Renew. Energy* **2014**, *62*, 388–398. [CrossRef]
53. Patel, A.M.; Singal, S.K. Economic analysis of integrated renewable energy system for electrification of remote rural area having scattered population. *Int. J. Renew. Energy Res.* **2018**, *8*, 523–539.
54. Yang, H.; Lu, L.; Zhou, W. A novel optimization sizing model for hybrid solar-wind power generation system. *Sol. Energy* **2007**, *81*, 76–84. [CrossRef]
55. Januar, R. Comparative Analysis of 20-MW Solar Thermal and PV Power Plant in Rongkop, Indonesia Using LCOE Simulation Method. *J. Clean Energy Technol.* **2017**, *5*, 383–388. [CrossRef]
56. Das, H.S.; Dey, A.; Wei, T.C.; Yatim, A.H.M. Feasibility analysis of standalone PV/wind/battery hybrid energy system for rural Bangladesh. *Int. J. Renew. Energy Res.* **2016**, *6*, 402–412.
57. Mousa, M.; Sagar, V.R.; Gajbhiye, V.T.; Kumar, R. Pesticides persistence in/on fresh and dehydrated brinjal. *J. Food Sci. Technol.* **2004**, *41*, 429–431.
58. Kamran, M.; Asghar, R.; Mudassar, M.; Ahmed, S.R.; Fazal, M.R.; Abid, M.I.; Zameer, M.Z. Designing and optimization of stand-alone hybrid renewable energy system for rural areas of Punjab, Pakistan. *Int. J. Renew. Energy Res.* **2018**, *8*, 2585–2597.
59. Dash, D.K.; Sadhu, P.K.; Subudhi, B. Spider monkey optimization (SMO) – lattice Levenberg–Marquardt recursive least squares based grid synchronization control scheme for a three-phase PV system. *Arch. Control. Sci.* **2021**, *31/3*, 707–730. [CrossRef]
60. Bouakkaz, A.; Haddad, S.; Martín-García, J.A.; Gil-Mena, A.J.; Jiménez-Castañeda, R. Optimal scheduling of household appliances in off-grid hybrid energy system using PSO algorithm for energy saving. *Int. J. Renew. Energy Res.* **2019**, *9*, 427–436.
61. Okonkwo, E.C.; Okwose, C.F.; Abbasoglu, S. Techno-economic analysis of the potential utilization of a hybrid PV-wind turbine system for commercial buildings in Jordan. *Int. J. Renew. Energy Res.* **2017**, *7*, 908–914.
62. Bai, S.; Rao, K.V.S. Design and integration of solar-biomass hybrid energy system for drip irrigation pumping. *J. Chem. Pharm. Sci.* **2014**, 247–248.
63. Adaramola, M.S.; Agelin-Chaab, M.; Paul, S.S. Analysis of hybrid energy systems for application in southern Ghana. *Energy Convers. Manag.* **2014**, *88*, 284–295. [CrossRef]
64. Kim, S.-K.; Jeon, J.-H.; Cho, C.-H.; Ahn, J.-B.; Kwon, S.-H. Dynamic modeling and control of a grid-connected hybrid generation system with versatile power transfer. *IEEE Trans. Ind. Electron.* **2018**, *55*, 1677–1688. [CrossRef]
65. Arivoli, S.; Karthikeyan, R.; Chitra, V. Implementation of Suitable Control Strategy for Improved Dynamics in Hybrid Grid Connected System. In Proceedings of the 2021 International Conference on Computer Communication and Informatics (ICCCI), Coimbatore, India, 27–29 January 2021; pp. 1–7. [CrossRef]
66. Elsayed, A.T.; Mohamed, A.A.; Mohammed, O.A. DC microgrids and distribution systems: An overview. *Electr. Power Syst.* **2015**, *119*, 407–417. [CrossRef]

67. Naresh, M.; Tripathi, R.K. Intelligent control strategy for power management in hybrid renewable energy system. In Proceedings of the 2019 Innovations in Power and Advanced Computing Technologies (i-PACT), Vellore, India, 22–23 March 2019; pp. 1–5. [CrossRef]
68. Soliman, M.A.; Hasanien, H.M.; Azazi, H.Z.; El-kholy, E.E.; Mahmoud, S.A. Hybrid ANFIS-GA-based control scheme for performance enhancement of a grid-connected wind generator. *IET Renew. Power Gener.* **2018**, *12*, 832–843. [CrossRef]
69. García, P.; García, C.A.; Fernández, L.M.; Llorens, F.; Jurado, F. ANFIS-Based Control of a Grid-Connected Hybrid System Integrating Renewable Energies Hydrogen and Batteries. *IEEE Trans. Ind. Inform.* **2014**, *10*, 1107–1117. [CrossRef]
70. Hornik, T.; Qing-Chang, Z. A current-control strategy for voltagesource inverters in microgrids based onH∞ and repetitive control. *IEEE Trans. Power Electron.* **2011**, *26*, 943–952. [CrossRef]
71. Lamichhane, A.; Zhou, L.; Yao, G.; Luqman, M. LCL Filter Based Grid-Connected Photovoltaic System with Battery Energy Storage. In Proceedings of the 2019 14th IEEE Conference on Industrial Electronics and Applications (ICIEA), Xi'an, China, 19–21 June 2019; pp. 1569–1574. [CrossRef]
72. Patel, N.; Kumar, A.; Gupta, N.; Ray, S.; Babu, B.C. Optimized PI-4VPI Current Controller for Three-Phase Grid-integrated Photovoltaic Inverter under Grid Voltage Distortions. *IET Renew. Power Gener.* **2019**, *14*, 779–792. [CrossRef]
73. Iqbal, M.M.; Kafiul, I. Design and Simulation of A PV System with Battery Storage Using Bidirectional DC-DC Converter Using Matlab Simulink. *Int. J. Sci. Technol. Res.* **2017**, *7*, 403.
74. Ruan, X.; Wang, X.; Pan, D.; Yang, D.; Li, W.; Bao, C. Introduction. In *Control Techniques for LCL-Type Grid-Connected Inverter*; Springer: Singapore, 2017; pp. 1–23.
75. Guo, Y.; LI, J.; Shi, T.; Wang, X.; Miao, M. Research on Coordinated Control Strategies of Hybrid PV/CSP Power Plants. In Proceedings of the 2018 China International Conference on Electricity Distribution (CICED), Tianjin, China, 17–19 September 2018; pp. 2077–2081. [CrossRef]
76. Seema; Singh, B. Grid synchronization control for an autonomous PV-wind-battery based microgrid. In Proceedings of the 2018 IEEMA Engineer Infinite Conference (eTechNxT), New Delhi, India, 13–14 March 2018; pp. 1–6. [CrossRef]
77. Naqvi, S.B.Q.; Kumar, S.; Singh, B. A PV-Battery System Operating in Islanded and Grid Connected Modes with Shunt Active Filter Capability. In Proceedings of the IEEE Industry Applications Society Annual Meeting 2020, Detroit, MI, USA, 10–16 October 2020; pp. 1–8.
78. Korada, N.; Mishra, M.K. Grid Adaptive Power Management Strategy for an Integrated Microgrid with Hybrid Energy Storage. *IEEE Trans. Ind. Electron.* **2017**, *64*, 2884–2892. [CrossRef]
79. Karimi-Ghartemani, M.; Khajehoddin, S.A.; Piya, P.; Ebrahimi, M. Universal Controller for Three-Phase Inverters in a Microgrid. *IEEE J. Emerg. Sel. Top. Power Electron.* **2016**, *4*, 1342–1353. [CrossRef]
80. Jia, W.; Ren, Y.; Xu, J.; Wu, X.; Zhou, L.; Qian, Z. Modeling and Control of Wind Storage Microgrid in Grid-connected and Off-grid Mode. In Proceedings of the 2020 IEEE Sustainable Power and Energy Conference (iSPEC), Chengdu, China, 23–25 November 2020; pp. 1419–1424. [CrossRef]
81. Tang, X.; Sun, Y.; Zhou, G.; Miao, F. Coordinated Control of Multi-Type Energy Storage for Wind Power Fluctuation Suppression. *Energies* **2017**, *10*, 1212. [CrossRef]
82. Hajiaghasi, S.; Salemnia, A.; Hamzeh, M. Hybrid energy storage system for microgrids applications: A review. *J. Energy Storage* **2019**, *21*, 543–570. [CrossRef]
83. Neira, S.; Pereda, J.; Rojas, F. Three-Port Full-Bridge Bidirectional Converter for Hybrid DC/DC/AC Systems. *IEEE Trans. Power Electron.* **2020**, *35*, 13077–13084. [CrossRef]
84. Perera, C.; Salmon, J.; Kish, G.J. DC/AC Voltage Sourced Converter with Auxiliary DC Port for Renewable Energy Applications. In Proceedings of the Energy Conversion Congress and Exposition (ECCE) 2020 IEEE, Detroit, MI, USA, 11–15 October 2020; pp. 1842–1849.
85. Neira, S.; Lizana, A.; Pereda, J. A Novel Three-Port NPC Converter for Grid-Tied Photovoltaic Systems with Integrated Battery Energy Storage. In Proceedings of the 2020 IEEE 11th International Symposium on Power Electronics for Distributed Generation Systems (PEDG), Dubrovnik, Croatia, 6 August 2020; pp. 104–109.
86. Shen, X.; Tan, D.; Shuai, Z.; Luo, A. Control techniques for bidirectional interlinking converters in hybrid microgrids: Leveraging the advantages of both ac and dc. *IEEE Power Electron. Mag.* **2019**, *6*, 39–47. [CrossRef]
87. Moradisizkoohi, H.; Elsayad, N.; Mohammed, O.A. A family of three-port three-level converter based on asymmetrical bidirectional half-bridge topology for fuel cell electric vehicle applications. *IEEE Trans. Power Electron.* **2019**, *34*, 11706–11724. [CrossRef]
88. Mahmood, H.; Michaelson, D.; Jiang, J. Decentralized power management of a PV/battery hybrid unit in a droop-controlled islanded microgrid. *IEEE Trans. Power Electron.* **2015**, *30*, 7215–7229. [CrossRef]
89. Kim, N.; Parkhideh, B. PV-battery series inverter architecture: A solar inverter for seamless battery integration with partial-power dc–dc optimizer. *IEEE Trans. Energy Convers.* **2019**, *34*, 478–485. [CrossRef]
90. Hamouda, N.; Benalla, H.; Hemsas, K.; Babes, B.; Petzoldt, J.; Ellinger, T.; Hamouda, C. Type-2 fuzzy logic predictive control of a grid connected wind power system with intergrated active power filter capabilities. *J. Power Electron.* **2017**, *17*, 1587–1599.
91. Birik, S.; Redif, S.; Khadem, S.K.; Basu, M. Improved harmonic suppression efficiency of single-phase APFs in distorted distribution systems. *Int. J. Electron.* **2016**, *103*, 232–246. [CrossRef]

92. Babes, B.; Rahmani, L.; Chaoui, A.; Hamouda, N. Design and experimental validation of a digital predictive controller for variable speed wind turbine systems. *J. Power Electron.* **2017**, *17*, 232–241. [CrossRef]
93. Hamouda, N.; Babes, B.; Kahla, S.; Soufi, Y.; Petzoldt, J.; Ellinger, T. Predictive Control of a Grid Connected PV System Incorporating Active power Filter functionalities. In Proceedings of the 2019 1st International Conference on Sustainable Renewable Energy Systems and Applications (ICSRESA), Tebessa, Algeria, 4–5 December 2019; pp. 1–6. [CrossRef]
94. Farhadi, P.; Sedaghat, M.; Sharifi, S.; Taheri, B. Power point tracking in photovoltaic systems by sliding mode control. In Proceedings of the 2017 10th International Symposium on Advanced Topics in Electrical Engineering (ATEE), Bucharest, Romania, 23–25 March 2017; pp. 781–785. [CrossRef]
95. Touil, S.-A.; Boudjerda, N.; Boubakir, A.; Boudouda, A. Sliding mode control of a grid-connected photovoltaic source via a three-phase inverter using incremental conductance MPPT. In Proceedings of the 2017 5th International Conference on Electrical Engineering—Boumerdes (ICEE-B), Boumerdes, Algeria, 29–31 October 2017; pp. 1–6. [CrossRef]
96. Saravanan, S.; Babu, N.R. Maximum power point tracking algorithms for photovoltaic system—A review. *Renew. Sustain. Energy Rev.* **2016**, *57*, 192–204. [CrossRef]
97. Arafa, O.; Mansour, A.; Sakkoury, K.; Atia, Y.; Salem, M. Realization of single-phase single-stage grid-connected PV system. *J. Electr. Syst. Inf. Technol.* **2017**, *4*, 1–9. [CrossRef]
98. Roy, T.; Mahmud, M. Active power control of three-phase grid-connected solar PV systems using a robust nonlinear adaptive backstepping approach. *Sol. Energy* **2017**, *153*, 64–76. [CrossRef]
99. Twaha, S.; Zhu, J.; Yan, Y.; Li, B.; Huang, K. Performance analysis of thermoelectric generator using dc-dc converter with incremental conductance based maximum power point tracking. *Energy Sustain. Dev.* **2017**, *37*, 86–98. [CrossRef]
100. Zhu, X.; Yu, T.; Zhang, Z.; Cao, Y.; Yang; Yi, Y. Sliding mode control of MIMO Markovian jump systems. *Automatica* **2016**, *68*, 286–293. [CrossRef]
101. Zouga, S.; Benchagra, M.; Abdallah, A. Backstepping Control Based on the PSO Algorithm for a Three-Phase PV System Connected to the Grid under Load Variation. In Proceedings of the Electrical and Information Technologies (ICEIT) 2020 International Conference, Rabat, Morocco, 4–7 March 2020; pp. 1–6.
102. Ndiaye, E.H.M.; Ndiaye, A.; Tankari, M.A.; Lefebvre, G. Adaptive Neuro-Fuzzy Inference System Application for the Identification of a Photovoltaic System and the Forecasting of Its Maximum Power Point. In Proceedings of the 2018 7th International Conference on Renewable Energy Research and Applications (ICRERA), Paris, France, 14–17 October 2018; pp. 1061–1067. [CrossRef]
103. Cordeiro, A.; Foito, D.; Pires, V. A PV Panel Simulator Based on a Two Quadrant DC/DC Power Converter with a Sliding Mode Controller. In Proceedings of the 4th International Conference on Renewable Energy Research and Application (ICRERA), Birmingham, UK, 20–23 November 2023; pp. 928–932.
104. Kirmani, S.; Jamil, M.; Akhtar, I. Effective low cost Grid-Connected Solar Photovoltaic System to Electrify the Small Scale industry/Commercial Building. In Proceedings of the International Journal of Renewable Energy Research (IJRER), San Diego, CA, USA, 5–8 December 2017; Volume 7, pp. 797–806.
105. Priyadarshi, N.; Anand, A.; Sharma, A.; Azam, F.; Singh, V.; Sinha, R. An Experimental Implementation and Testing of GA based Maximum Power Point Tracking for PV System under Varying Ambient Conditions Using dSPACE DS 1104 Controller. *Int. J. Renew. Energy Res.* **2017**, *7*, 255–265.
106. Boukenoui, R.; Bradai, R.; Mellit, A.; Ghanes, M.; Salhi, H. Comparative Analysis of P&O Modified Hill Climbing-FLC and Adaptive P&O-FLC MPPTs for Microgrid Standalone PV System. In Proceedings of the 4th International Conference on Renewable Energy Research and Application (ICRERA), Birmingham, UK, 20–23 November 2016; pp. 1095–1099.
107. Shabaan, S.; El-Sebah, M.; Bekhit, P. Maximum Power Point Tracking for photovoltaic solar pump based on ANFIS tuned system. *J. Electr. Syst. Inf. Technol.* **2018**, *5*, 11–22. [CrossRef]
108. Amara, K.; Fekik, A.; Hocine, D.; Bakir, M.L.; Bourennane, E.B.; Malek, T.A.; Malek, A. Improved Performance of a PV Solar Panel with Adaptive Neuro Fuzzy Inference System ANFIS based MPPT. In Proceedings of the 2018 7th International Conference on Renewable Energy Research and Applications (ICRERA), Paris, France, 14–17 October 2018; pp. 1098–1101. [CrossRef]
109. Yilmaz, U.; Kircay, A.; Borekci, S. PV system fuzzy logic MPPT method and PI control as a charge controller. *Renew. Sustain. Energy Rev.* **2018**, *81*, 994–1001. [CrossRef]
110. Singh, S.N. Selection of non-isolated DC-DC converters for solar photovoltaic system. *Renew. Sustain. Energy Rev.* **2017**, *76*, 1230–1247.
111. Valarezo, D.; Peralta-Sevilla, A.; Icaza, D.; Méndez, G.; Ochoa, P.C.; Espinoza, J.R. Special Outlook of Energy Optimization for A Bioecological Infrastructure. In Proceedings of the 2021 10th Renewable Energy Research and Application (ICRERA)International Conference, Istanbul, Turkey, 26–29 September 2021; pp. 250–257.
112. Iqbal, A.; Abu-Rub, H.; Ahmed, S.M. Adaptive neuro-fuzzy inference system based maximum power point tracking of a solar PV module. In Proceedings of the 2010 IEEE International Energy Conference, Manama, Bahrain, 18–22 December 2010; pp. 51–56. [CrossRef]
113. Hichami, N.E.L.; Abbou, A.; Rhaili, S.E.; Ziouh, A.; Marhraoui, S. Grid Connected Photovoltaic System using a Fuzzy Logic Control Approach. In Proceedings of the 2018 IEEE 59th International Scientific Conference on Power and Electrical Engineering of Riga Technical University (RTUCON), Riga, Latvia, 11 December 2018; pp. 1–5. [CrossRef]

114. Zerouali, M.; El Ougli, A.; Tidhaf, B.; Zrouri, H. Fuzzy logic MPPT and battery charging control for photovoltaic system under real weather conditions. In Proceedings of the 2020 IEEE 2nd International Conference on Electronics, Control, Optimization and Computer Science (ICECOCS), Kenitra, Morocco, 2–3 December 2020. [CrossRef]
115. Assahout, S.; El Aissaoui, H.; El Ougli, A.; Tidhaf, B.; Zrouri, H. A Neural Network and Fuzzy Logic based MPPT Algorithm for Photovoltaic Pumping System. *Int. J. Power Electron. Drive Syst.* **2018**, *9*, 1823. [CrossRef]
116. Motahhir, S.; El Hammoumi, A.; El Ghzizal, A. Photovoltaic system with quantitative comparative between an improved MPPT and existing INC and P&O methods under fast varying of solar irradiation. *Energy Rep.* **2018**, *4*, 341–350.
117. Arunkumari, T.; Indragandhi, V.; Sreejith, S. Topologies of a DC–DC Converter for Micro-Grid Application and Implementation of Parallel Quadratic Boost Converter. *Adv. Smart Grid Renew. Energy* **2018**, *435*, 633–644.
118. Gude, S.; Chu, C.C. Three-phase PLLs by using frequency adaptive multiple delayed signal cancellation prefilters under adverse grid conditions. *IEEE Trans. Ind. Appl.* **2018**, *54*, 3832–3844. [CrossRef]
119. Miqoi, S.; El Ougli, A.; Boutouba, M.; Tidhaf, B. Fuzzy sliding mode control for maximum power point tracking of a photovoltaic pumping system. *J. Electr. Syst.* **2017**, *13*, 95–114.
120. Aidoud, M.; Feraga, C.E.; Bechouat, M.; Sedraoui, M.; Kahla, S. Development of photovoltaic cell models using fundamental modeling approaches. *Energy Procedia* **2019**, *162*, 263–274. [CrossRef]
121. Babu P, N.; Guerrero, J.M.; Siano, P.; Peesapati, R.; Panda, G. An Improved Adaptive Control Strategy in Grid-Tied PV System with Active Power Filter for Power Quality Enhancement. *IEEE Syst. J.* **2021**, *15*, 2859–2870. [CrossRef]
122. Kumar, V.; Pandey, A.S.; Sinha, S.K. Grid integration and power quality issues of wind and solar energy systems: A review. In Proceedings of the International Conference on Emerging Trends in Electrical, Electronics and Sustainable Energy Systems 2016, Sultanpur, India, 11–12 March 2016; pp. 71–80.
123. Kumar, V.N.; Babu, P.N.; Kiranmayi, R.; Siano, P.; Panda, G. Improved power quality in a solar PV plant integrated utility grid by employing a novel adaptive current regulator. *IEEE Syst. J.* **2020**, *14*, 4308–4319. [CrossRef]
124. Babu, P.N.; Choudhury, B.K.; Kar, B.; Halder, B. Modelling of a hybrid active power filter for power quality improvement using synchronous reference frame theory. *Int. J. Eng. Tech. Res.* **2017**, *6*, 369–374.
125. Ibrahim, S.A.; Nasr, A.; Enany, M.A. Maximum Power Point Tracking Using ANFIS for a Reconfigurable PV-Based Battery Charger Under Non-Uniform Operating Conditions. *Access IEEE* **2021**, *9*, 114457–114467. [CrossRef]
126. Pradhan, S.; Hussain, I.; Singh, B.; Panigrahi, B.K. Modified VSS-LMS-based adaptive control for improving the performance of a single-stage PV integrated grid system. *IET Sci. Meas. Technol.* **2017**, *11*, 388–399. [CrossRef]
127. Chilipi, R.S.R.; Al Sayari, N.; Al Hosani, K.H.; Beig, A.R. Adaptive notch filter-based multipurpose control scheme for grid-interfaced three-phase four-wire DG inverter. *IEEE Trans. Ind. Appl.* **2017**, *53*, 4015–4027. [CrossRef]
128. Xin, Z.; Wang, X.; Qin, Z.; Lu, M.; Loh, P.C.; Blaabjerg, F. An improved second-order generalized integrator based quadrature signal generator. *IEEE Trans. Power Electron.* **2016**, *31*, 8068–8073. [CrossRef]
129. Rodriguez, P.; Luna, A.; Candela, I.; Mujal, R.; Teodorescu, R.; Blaabjerg, F. Multiresonant frequency-locked loop for grid synchronization of power converters under distorted grid conditions. *IEEE Trans. Ind. Electron.* **2011**, *58*, 127–138. [CrossRef]
130. Liu, Z.; Mohammadzadeh, A.; Turabieh, H.; Mafarja, M.; Band, S.S.; Mosavi, A. A New Online Learned Interval Type-3 Fuzzy Control System for Solar Energy Management Systems. *IEEE Access* **2021**, *9*, 10498–10508. [CrossRef]
131. Chakir, A.; Tabaa, M.; Moutaouakkil, F.; Medromi, H.; Julien-Salame, M.; Dandache, A.; Alami, K. Optimal energy management for a grid connected PV-battery system. *Energy Rep.* **2020**, *6*, 218–231. [CrossRef]
132. Guo, Y.; Dai, X.; Jermsittiparsert, K.; Razmjooy, N. An optimal configuration for a battery and PEM fuel cell-based hybrid energy system using developed krill herd optimization algorithm for locomotive application. *Energy Rep.* **2020**, *6*, 885–894. [CrossRef]
133. Hamzeh, M.; Farhangi, S.; Farhangi, B. A new control method in PV grid connected inverters for anti-islanding protection by impedance monitoring. In Proceedings of the 2008 11th Workshop on Control and Modeling for Power Electronics, Zurich, Switzerland, 17–20 August 2008; pp. 1–5. [CrossRef]
134. Awasthi, A.; Shukla, A.K.; Dondariya, M.M.S.R.C.; Shukla, K.N.; Porwal, D.; Richhariya, G. Review on sun tracking technology in solar PV system. *Energy Rep.* **2020**, *6*, 392–405. [CrossRef]
135. Zaouche, F.; Rekioua, D.; Gaubert, J.-P.; Mokrani, Z. Supervision and control strategy for photovoltaic generators with battery storage. *Int. J. Hydrog. Energy* **2017**, *42*, 19536–19555. [CrossRef]
136. Zhang, R.; Hredzak, B. Nonlinear sliding mode and distributed control of battery energy storage and photovoltaic systems in AC microgrids with communication delays. *IEEE Trans. Ind. Informat.* **2019**, *15*, 5149–5160. [CrossRef]
137. Errouha, M.; Derouich, A.; Motahhir, S.; Zamzoum, O.; El Ouanjli, N.; El Ghzizal, A. Optimization and control of water pumping PV systems using fuzzy logic controller. *Energy Rep.* **2019**, *5*, 853–865. [CrossRef]
138. Parvaneh, M.H.; Khorasani, P.G. A new hybrid method based on fuzzy logic for maximum power point tracking of photovoltaic systems. *Energy Rep.* **2020**, *6*, 1619–1632. [CrossRef]
139. Mosavi, M.S.S.S.A.; Qasem, S.N.; Mohammadzadeh, A. Fractional-order fuzzy control approach for photovoltaic/battery systems under unknown dynamics variable irradiation and temperature. *Electronics* **2020**, *9*, 1455. [CrossRef]
140. Pradhan, S.S.; Pradhan, R.; Subudhi, B. Design and Analysis of an H∞ Controller for a Single Phase Grid Connected Photovoltaic System with Parametric Uncertainties. In Proceedings of the 2019 Second International Conference on Advanced Computational and Communication Paradigms (ICACCP), Gangtok, India , 25–28 February 2019; pp. 1–6. [CrossRef]

141. Mao, W.; Dai, N.; Li, H. Economic dispatch of microgrid considering fuzzy control based storage battery charging and discharging. *J. Electr. Syst.* **2019**, *15*, 417–428.
142. Li, X.; Yan, H. Fuzzy logic-based coordinated control method for multi-type battery energy storage systems. *Artif. Intell. Rev.* **2018**, *49*, 227–243. [CrossRef]
143. Kim, J.-C.; Huh, J.-H.; Ko, J.-S. Improvement of MPPT control performance using fuzzy control and VGPI in the PV system for micro grid. *Sustainability* **2019**, *11*, 5891. [CrossRef]
144. Wang, Y.; Ahn, C.K.; Yan, H.; Xie, S. Fuzzy control and filtering for nonlinear singularly perturbed Markov jump systems. *IEEE Trans. Cybern.* **2021**, *51*, 297–308. [CrossRef]
145. Noman, A.M.; Alkuhayli, A.; Al-Shamma'a, A.A.; Addoweesh, K.E. Hybrid MLI Topology Using Open-End Windings for Active Power Filter Applications. MDPI. *Energies* **2022**, *15*, 6434. [CrossRef]
146. Panati, P.U.; Ramasamy, S.; Ahsan, M.; Haider, J.; Rodrigues, E.M.G. Indirect Effective Controlled Split Source Inverter-Based Parallel Active Power Filter for Enhancing Power Quality. *Electronics* **2021**, *10*, 892. [CrossRef]
147. Jayaram, J.; Srinivasan, M.; Prabaharan, N.; Senjyu, T. Design of Decentralized Hybrid Microgrid Integrating Multiple Renewable Energy Sources with Power Quality Improvement. *Sustainability* **2022**, *14*, 7777. [CrossRef]
148. Chowdhury, M. Dual-loop H∞controller design for a grid-connected single-phasephotovoltaic system. *Elseiver Solar Energy* **2016**, *139*, 640–649. [CrossRef]
149. Jendoubi, A.; Tlili, F.; Bacha, F. Sliding mode control for a grid connected PV-system using interpolation polynomial MPPT approach. *Sci. Direct.* **2019**, *167*, 202–218. [CrossRef]
150. Das, S.R.; Ray, P.K.; Sahoo, A.K.; Ramasubbareddy, S.; Babu, T.S.; Kumar, N.M.; Elavarasan, R.M.; Mihet-Popa, L. A Comprehensive Survey on Different Control Strategies and Applications of Active Power Filters for Power Quality Improvement. *Energies* **2021**, *14*, 4589. [CrossRef]
151. Zhao, Y.; An, A.; Xu, Y.; Wang, Q.; Wang, M. Model Predictive control of grid connected PV power generation system considering optimal MPPT control of PV modules. *Prot. Control Mod. Power Syst.* **2021**, *6*, 32. [CrossRef]
152. Huang, L.; Chen, D.; Lai, C.S.; Huang, Z.; Zobaa, A.F.; Lai, L.L. A distributed optimization model for mitigating three-phase power imbalance with electric vehicles and grid battery. *Electr. Power Syst. Res.* **2022**, *210*, 108080. [CrossRef]
153. Shen, Z.; Jiang, D.; Zou, J.; Liu, Z.; Ma, C. Current-balance mode-based unified common-mode voltage elimination scheme for dual three-phase motor drive system. *IEEE Trans. Ind. Electron.* **2022**, *69*, 12575–12586. [CrossRef]
154. Aggarwal, S.; Garg, N.; Kaur, G. Performance evaluation of various dispersion compensation modules. *Wirel. Pers. Commun.* **2022**, *123*, 1–15. [CrossRef]